AD-A013 557

DEFENSE NUCLEAR AGENCY REACTION RATE HANDBOOK. SECOND EDITION. REVISION NUMBER 4, MARCH 1975

M. H. Bortner, et al

General Electric Company

Prepared for:

Defense Nuclear Agency

March 1975

MEMORANDUM

To: Recipients of the DNA Reaction Rate Handbook (DNA 1948H)

From: The Editors

Subject: Revision Number 4

Enclosed herewith you will find a copy of Revision Number 4 to the Handbook. It comprises minor corrections to individual pages within Chapters 1, 9, 11, 12, and 14, and some important changes of content in Chapter 10.

You should immediately and carefully substitute the enclosed items into your copy of the Handbook, discarding the pages which they replace.

You should also enter on page iii in front of your Handbook the following information: Revision Number 4; Date of Issue—March 1975; Date of Receipt—whatever day you receive this; and sign your name in the last column.

Revision Number 5 and several following revisions are expected out later this year. Thank you for your cooperation.

One of the forthcoming revisions is slated to be devoted entirely to the updating of Appendices, in line with all other revisions which will have been issued prior to it.

DISCLAIMER NOTICE

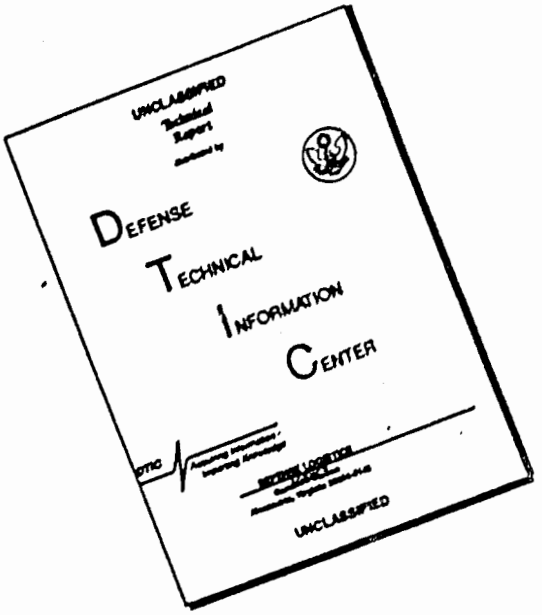

THIS DOCUMENT IS BEST QUALITY AVAILABLE. THE COPY FURNISHED TO DTIC CONTAINED A SIGNIFICANT NUMBER OF PAGES WHICH DO NOT REPRODUCE LEGIBLY.

Copy No.____

REVISION NUMBER 4, MARCH 1975

DNA 1948H
(Formerly DASA 1948)

DEFENSE NUCLEAR AGENCY

REACTION RATE HANDBOOK
SECOND EDITION

Editors-in-Chief:

Dr. M.H. Bortner
Dr. T. Baurer

MARCH 1972

Project Officer: Dr. C.A. Blank

APPROVED FOR PUBLIC RELEASE, DISTRIBUTION UNLIMITED

Organized by General Electric Space Sciences Laboratory
for Defense Nuclear Agency Under Contracts
DASA 01-70-C-0082 and DASA 01-71-C-0145

This effort supported by Defense Nuclear Agency
NWED Subtask Code HD028, Work Unit 11

Published by DASIAC
DoD Nuclear Information and Analysis Center
General Electric, TEMPO
Santa Barbara, California

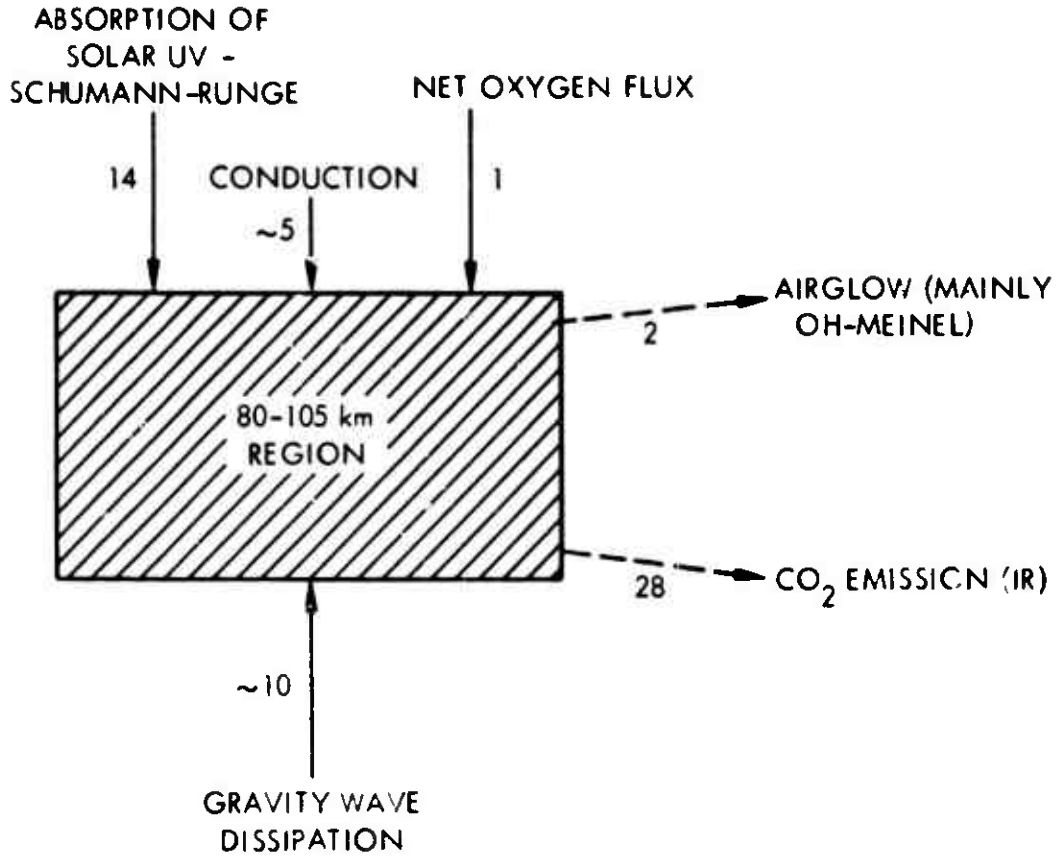

Figure 4-6. Schematic heat budget constituents between 80 and 105 km. (From Reference 4-6.)

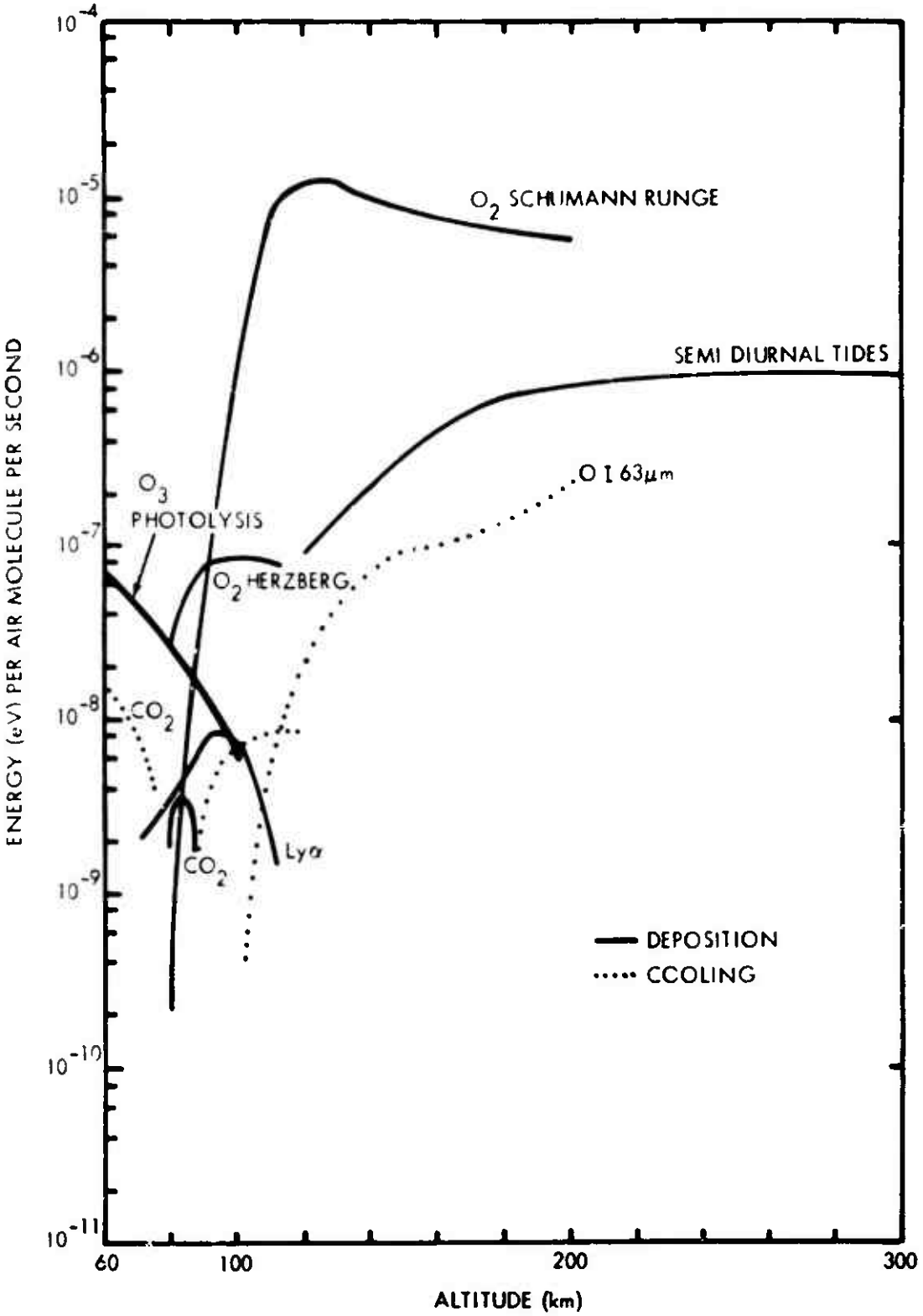

Figure 4-7. Altitude dependence of energy absorption and emission.

Table 9-5. (Cont'd.)

	q (photons cm^{-3} sec^{-1})	d (layer, cm)	h_q (km)	Remarks
1	1.1×10^{-4}			Nightglow radiation could be either or both.
2	1.7×10^{-5}			
3				
4	2.6×10^{-6}			
5				
6	2.1×10^{-3}	$(4.5 \times 10^{-18} [N_2])$		
7	1.0×10^{-4}			
8				
9				Lyman-Birge-Hopfield
10				
11	4.0×10^{-6}			γ bands; β for 1-0 band
12				2nd positive
13				Vegard-Kaplan
14				Herzberg
15				
16	0.1			β $He(^3S)$
17	.050	$10^{-8} [N_2]$	46	[illegible] active
18	0.3, 0.15			
19				
20	(6×10^{-11})		~200	Also quenched by electrons
21				Continuum
22	(1×10^{-11})	$3 \times 10^{-8} [O_2]$	94	2972Å (5%)
23	0.80		50	
24	(4.5×10^{-10})	$9.8 \times 10^{-6} [O_2]$	340	
25	2.6×10^{-6}			
26	16			May be of artificial origin
27	6.3×10^{-9}	$\approx 5 \times 10^{-3} [O_3]$	90	Atmospheric
28	1.67			
29			37	1st positive
30			37	1st positive
31	16.8		~400	Scattered in $He(^3S)$; h_q for its destruction.
32	.042	2.8×10^{-8}		Meinel; β,δ for 1-0 band (9500Å)
33	(9.4×10^{-11})	$9.5 \times 10^{-3} [O_3]$	75	IR Atm; 0-1 band 1.58μ; Meinel bands 1.9μ
34				Meinel; 4.5μ to 3816Å

Table 9-6. Fluorescence efficiencies measured in auraras.

Wavelength A	Transition	Fluorescence Efficiency	Comments	Reference
3914	$N_2^+(0,0)\,B^2\Sigma-X^2\Sigma$ 1st neg.	4.1×10^{-3}	Rocket photometer and electron energy detector	Miller et al. 9-103
		7×10^{-3}	Satellite photometer and particle detector	Meyerott and Evans 9-21
4278	$N_2^+(0,0)\,B^2\Sigma-X^2\Sigma$ 1st neg.	$(11\pm4)\times10^{-4}$	Ground photometer, rocket electran detector	Bryant et al. 9-104
Labaratary derived values used extensively in ratio measurements				
3914	$N_2^+(0,0)\,B^2\Sigma-X^2\Sigma$ 1st neg.	3.7×10^{-3}	Laboratory value	Dalgarno et al. 9-105
4278		1.0×10^{-3}	From 3914 value and branching ratio	Dalgarno et al. 9-105
4709		2.2×10^{-4}	From 3914 value and branching ratio	Dalgarno et al. 9-105
1180	$N_2(0,13)\,h\,^1\Sigma-X\,^1\Sigma$ W-K	3×10^{-5}	Ratio with 3914	Miller et al. 9-103
1200	N I $^4P-^4S$	4×10^{-3}	Ratio with 3914	Theobald and Peek 9-106
		7×10^{-4}	Ratio with 3914	Miller et al. 9-103
1216	H Lyman α	5×10^{-2}	Satellite photometer, estimate of proton flux	Metzger and Clark 9-107
1240	N_2 BH(5, 11)	7×10^{-5}	Ratio with 3914	Miller et al. 9-103
	N_2 BH or N I	6×10^{-4}	Ratio with 3914	Theobald and Peek 9-106
1273	N_2 LBH(6, 0) $a\,^1\Pi-X\,^1\Sigma$	1.1×10^{-4}	Ratio with 3914	Miller et al. 9-103
1325	N_2 LBH(4, 0)	2.6×10^{-4}	Ratio with 3914	Miller et al. 9-103
1339	N_2 LBH(5, 1)	5×10^{-5}	Ratio with 3914	Miller et al. 9-103
1354	N_2 LBH(3, 0)	5×10^{-4}	Ratio with 3914	Miller et al. 9-103
1356	O I $^5S-^3P$	3×10^{-4}	Ratio with 3914	Miller et al. 9-103
		3×10^{-3}	Ratio with 3914	Theobald and Peek 9-106
1382	N_2 LBH(5,2)	7.5×10^{-5}	Ratio with 3914	Miller, et al. 9-103

Table 9-6. (Cont'd.)

Wavelength A	Transition	Fluorescence Efficiency	Comments	Reference	
1384	N_2 LBH(2,0)	4×10^{-4}	Ratio with 3914	Miller et al.	9-103
		1×10^{-4}	Ratio with 3914	Theobald and Peek	9-106
1412	N_2 LBH(4,2)	2×10^{-4}	Ratio with 3914	Miller et al.	9-103
1416	N_2 LBH(1,0)	2×10^{-4}	Ratio with 3914	Miller et al.	9-103
1426	N_2 LBH(5,3)	7×10^{-5}	Ratio with 3914	Miller et al.	9-103
1430	N_2 LBH(2,1)	3×10^{-4}	Ratio with 3914	Miller et al.	9-103
1444	N_2 LBH(3,2)	2×10^{-4}	Ratio with 3914	Miller et al.	9-103
1464	N_2 LBH(1,1)	3×10^{-4}	Ratio with 3914	Miller et al.	9-103
		8×10^{-4}	Ratio with 3914	Theobald and Peek	9-106
1473	N_2 LBH(5,4)	8×10^{-5}	Ratio with 3914	Miller et al.	9-103
1493	N_2 LBH(3,3)	1×10^{-4}	Ratio with 3914	Miller et al.	9-103
1493	N I $^2P-^2D$	3×10^{-4}	Ratio with 3914	Miller et al.	9-103
		1×10^{-3}	Ratio with 3914 (>110km)	Theobald and Peek	9-106
1508	N_2 LBH(4,4)	4×10^{-5}	Ratio with 3914	Miller et al.	9-103
1515	N_2 LBH(1,2)	8×10^{-5}	Ratio with 3914	Miller et al.	9-103
1530	N_2 LBH(2,3)	1×10^{-4}	Ratio with 3914	Miller et al.	9-103
		5×10^{-4}	Ratio with 3914	Theobold ond Peek	9-106
1555	N_2 LBH(0,2)	5×10^{-4}	Ratio with 3914	Theobald and Peek	9-106
Total N_2 BH system		6×10^{-3}	Ratio with 3914 and BH(5,11)	Miller et al.	9-103
1205-2602 Total N_2 LBH system ($a^1\Pi-X^1\Sigma$)		2×10^{-2} (>110km)	Ratio with 3914	Theobald and Peek	9-106
		3×10^{-2} (>130km)	Ratio with 3914	Theobald ond Peek	9-106
		7×10^{-3}	Ratio with 3914	Miller et al.	9-103

Table 9-6. (Cont'd.)

Wavelength A	Transition	Fluorescence Efficiency	Comments	Reference	
2333-5060	N_2 Vegard-Kaplan bands $A^3\Sigma$-$X^1\Sigma$	7×10^{-3}	Ratio with N_2^+ (first neg.)	Chamberlain	9-108
	($v^1 = 0$) N_2 Vegard-Kaplan	1.0×10^{-3}	Ratio with 4278, from 100 km upward	Sharp	9-109
	($v^1 = 1$) N_2 Vegard-Kaplan	7×10^{-4}	Ratio with 4278, from 100 km upward	Sharp	9-109
2470	O II ^2P-^4S	8×10^{-5}	Branching ratio with 7319-30	Chamberlain	9-108
2972	O I ^1S-^3P	2.2×10^{-4}	Branching ratio with 5577	Chamberlain	9-108
3371	N_2(0, 0) (2nd pos.)	2.5×10^{-3}	Ratio with 4278	Sharp	9-109
3466	N I ^2P-^4S	8×10^{-5}	Ratio with 6300 OI	Dick	9-110
3727	O II ^2D-^4S	2×10^{-5}	Ratio with N_2^+ (1st neg.)	Chamberlain	9-108
4059	N_2 2nd pos. C $^3\Pi$-B $^3\Pi$	1.6×10^{-4}	Ratio with 3914	Theobald and Peek	9-106
3116-4574	Total N_2 2nd pos.	5×10^{-3}	Ratio with 3914	Theobald and Peek	9-106
		3.5×10^{-3}	Ratio with N_2^+ (1st neg.)	Chamberlain	9-108
4368	O I ^3P-^3S	1.6×10^{-5}	Ratio with 4278 N_2^+	Dick	9-110
4415	O II ^2D-^2P	1.6×10^{-5}	Ratio with 4368	Chamberlain	9-108
4861	H_β	9×10^{-5}	Protons in past breakup display	Reasoner et al.	9-111
		3.0×10^{-4}	Ratio with 3914	Eather	9-112
		2.4×10^{-4}	Ratio with 4709	Eather	9-112
		3.3×10^{-4}	Proton component in aurora	McIlwain	9-113

Table 9-6. (Cont'd.)

Wavelength A	Transition	Fluorescence Efficiency	Comments	Reference	
5200	N I ^2D-^4S	3.3×10^{-5}	Ratio with 4278	Eather and Mende	9-10
		6.6×10^{-4}	Ratio with 4278 soft particles	Eather and Mende	9-10
5577	O I ^1S-^1D	4.2×10^{-3}	Ratio with 3914 (K_p 1)	Sandford	9-114
		3.1×10^{-3}	Ratio with 3914 (K_p 4±2)	Sandford	9-114
		3.9×10^{-3}	Ratio with 4278	Mende and Eather	9-115
		8.3×10^{-3}	Ratio with 3914	Theobald and Peek	9-106
		$(6\pm2)\times10^{-4}$	Electrons from rockets, ground-based photometer	Bryant et al.	9-104
		2.0×10^{-3}	Ratio with 4861 in pratan arc	Eather and Mende	9-10
5893	Na	2×10^{-5}	Upper limit and applicable anly ta law-lying displays such c: type B auroras	Chamberlain	9-108
6300	O I ^1D-^3P	8×10^{-4}	Ratio with 4278	Eather ar.d Mende	9-10
		4×10^{-4}	Ratio with 3914	Theobald and Peek	9-106
		7×10^{-3}	Ratia with 4278 soft particles	Eather and Mende	9-10
		5.6×10^{-4}	Ratio with 4861 in proton arc	Chamberlain	9-108
6364	O I ^1D-^3P	1.2×10^{-4}	Branching ratio with 6300	Chamberlain	9-108
6563	H_α	4.5×10^{-3}	Proton and H_α in proton arc	Ramick and Sharp	9-116
7319-30	O II ^2P-^2D	1.5×10^{-4}	Ratio with 5577	Chamberlain	9-108
7036-15, 748	N_2^+ Meinel bands $A^2\Pi$-$X^2\Sigma$	3×10^{-2}	Ratio with N_2^+ (1st neg.)	Chamberlain	9-108

Table 9-6. (Cont'd.)

Wavelength A	Transition	Fluorescence Efficiency	Comments	Reference	
7684-8598	O_2 atmospheric bands				
	$b\,^1\Sigma - X\,^3\Sigma$	5×10^{-3}	Ratio with N_2^+ (1st neg.)	Chamberlain	9-108
	O_2 (1, 1) atmospheric	3×10^{-4}	Ratio with 5577 (17)	Omhalt	9-117
	O_2 infrared atmaspheric $a\,^1\Delta - X\,^3\Sigma$	8×10^{-4}	Ratio with N_2^+ (1st neg.)	Chamberlain	9-108
5296-6419	O_2^+ (1st neg.) bands $b\,^4\Sigma - a\,^4\Pi$	2×10^{-4}	Ratio with N_2^+ (1st neg.)	Chamberlain	9-108
7774	O I $^5P - ^5S$	2.5×10^{-4}	Ratio with 5577	Omhalt	9-117
8446	O I $^3P - ^3S$	3.7×10^{-4}	Ratio with 5577	Omhalt	9-117
10400	N I $^2P - ^2D$	2×10^{-3}	Ratio with 5577	Chamberlain	9-108

Here, K'_{01} (sec^{-1}) and K'_{10} (sec^{-1}) are the collisional excitation and deexcitation rates, respectively, $[X(i)]$ is the number density (cm^{-3}) of species X in vibrational state i, and A_{10} (sec^{-1}) is the Einstein coefficient for the transition (cf. Table 11-1). If Z_{ij} is the number of collisions required to bring about one transition from state i to state j, and N is the number of collisions per second experienced by a molecule at a given altitude, then $K'_{ij} = N/Z_{ij}$. For the example given, $K'_{10} = N/Z >> A_{10}$ is the condition to be met if radiative loss is not to disrupt LTE. In that case $[X(1)]/[X(0)]$ is given by the Boltzmann factor, $\exp[-\theta/T]$, where T is the kinetic temperature and θ is the characteristic temperature $h\nu_o/k$ of the mode. When $T << \theta$, the reciprocal of K'_{10} is a good approximation to the relaxation time for the system; it applies about as well for a system of many harmonic oscillators (Reference 11-17).

Failure of K'_{10} to dominate A_{10} implies $[X(1)]/[X(0)] < \exp[-\theta/T]$, $T_{vib} < T_{kinetic}$, and therefore a condition where the volume emission rate in an optically thin atmosphere is subject to one variety of collision-limiting. For most species this condition has its onset somewhere above 70 km, the actual altitude depending on where in the atmosphere $N/Z_{10} \sim A_{10}$. Values of Z_{10} for CO_2 and H_2O are listed in Table 11-2.

The emission features of the spectra shown in Figures 11-1 and 11-2 are attributable to thermal radiation from chemically stable species in the atmosphere. For important minor species like O_3 at 9.6 μm and CO_2 at 15 μm, the atmosphere is optically thick to the radiation. The surface brightness of the atmosphere at these wavelengths approaches that of a blackbody at the local kinetic temperature. To calculate the brightness of thermally excited transitions for which the atmosphere is not optically thick, given a specific slant path, requires a knowledge of the number-density profile of the emitting species along the line of sight, as well as the atmospheric temperature in each volume element along the optical path. Then within each such volume element, again using the 1, 0 transition of species X as an example:

$$I_{vol} = \frac{[X]\, A_{10} \exp[-\theta/T]}{Q_V} \text{ photons cm}^{-3} \text{ sec}^{-1} , \qquad (11\text{-}3)$$

where I_{vol} is the volume emission rate, Q_V is the vibrational partition function for species X, and $[X]$ is the concentration of species

Table 11-2. Collisional Excitation Parameters.

Originally Excited Species	Bond Origin Wave Number, ν_o (cm^{-1})	Characteristic Temperature, $\theta = \frac{h\nu_o}{k}$ (K)	No. of Collisions Required to Bring About V-V Exchange:		No. of Collisions Required to Bring About T-V Exchange:		Reference[b]
			Z_{01}^{10}[a]	With Collision Partner	Z_{10}^{o}	With Collision Partner	
CO_2	667	959	—	—	4×10^5	N_2	11-20
CO_2	2349	3380	7×10^2	N_2	—	—	11-20
H_2O	1595	2295	$\sim 5 \times 10^3$	O_2	$\sim 2 \times 10^4$	Air	11-20
NO	1876	2700	5×10^5	N_2	—	—	11-18
NO(A)	2341	3371	7.9×10^2	N_2	—	—	11-18
CO	2143	3080	4.5×10^6	O_2	—	—	11-18
O_2	1556	2228	—	—	—	—	11-18
N_2	2331	3336	—	—	—	—	11-17

Notes:

[a] The Z-values relate to ~300 K.

[b] Reference 11-17 derives the theoretical basis for calculating relaxation rates at other temperatures and References 11-18 and 11-20 compile much of the pertinent data.

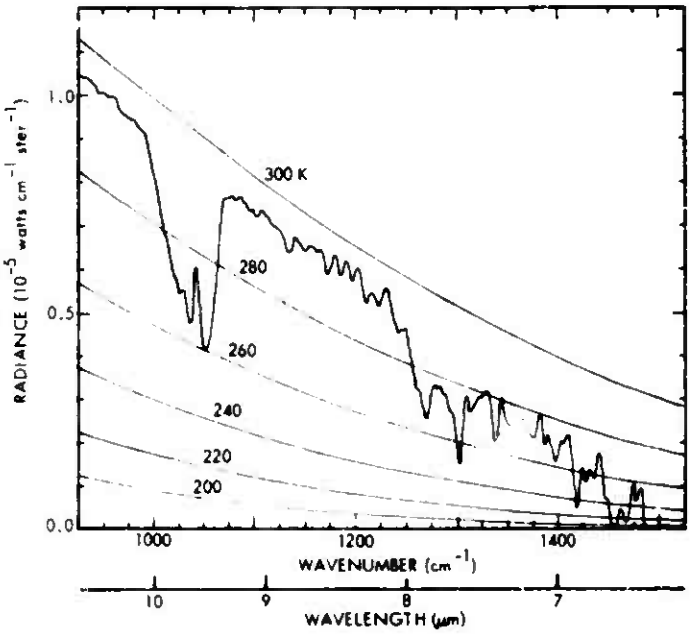

Figure 11-5. Earthshine in the 1000-1450 cm^{-1} region (Reference 11-41).

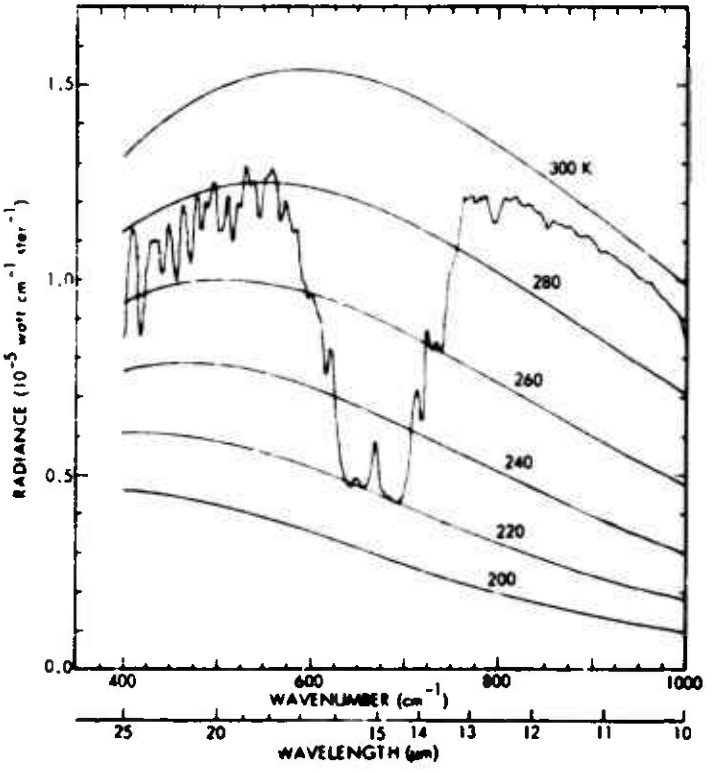

Figure 11-6. Earthshine in the 400-1000 cm^{-1} region (Reference 11-41).

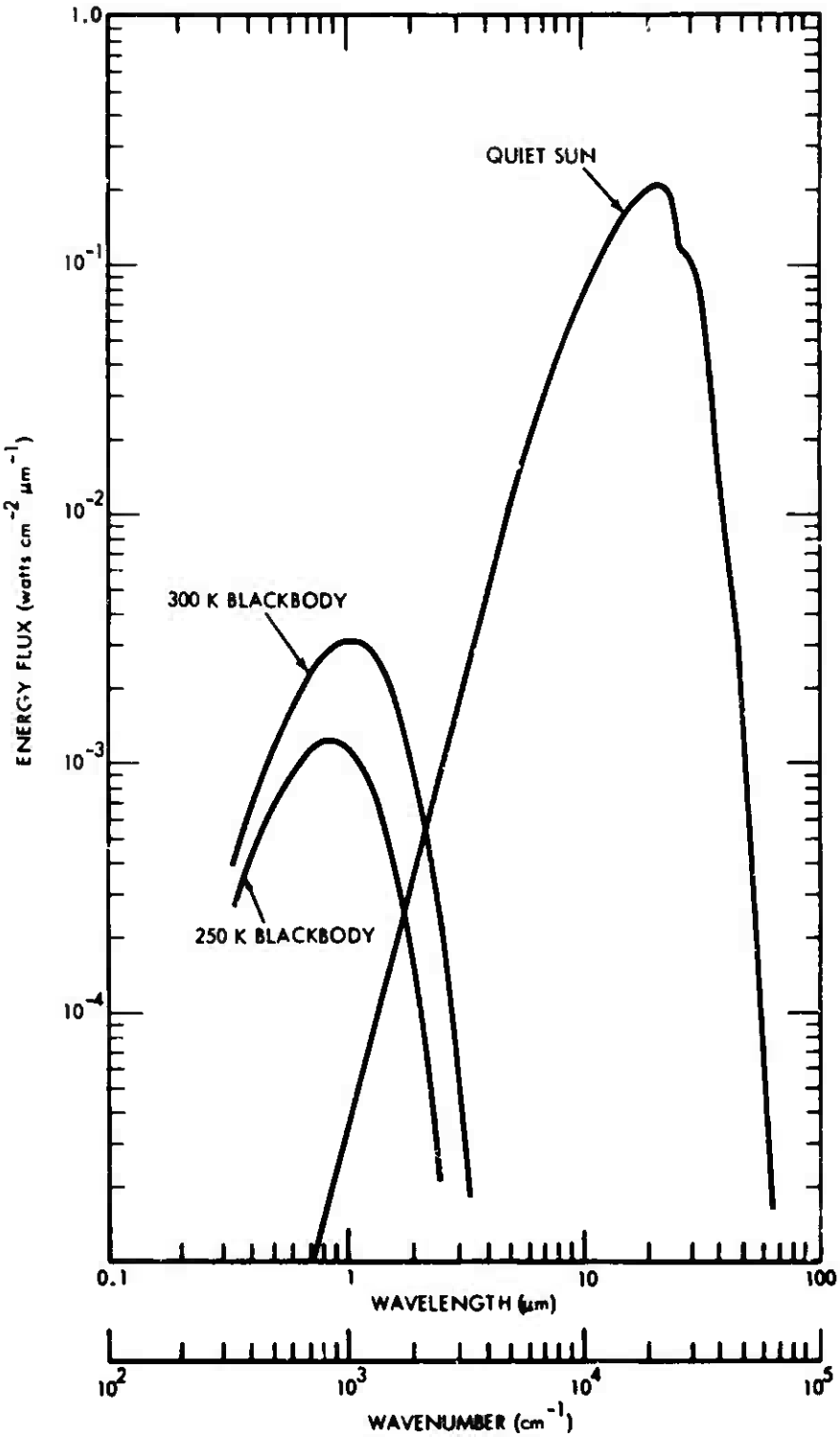

Figure 11-7. Irradionce at the top of the atmosphere, for quiet sun ond two blackbody sources.

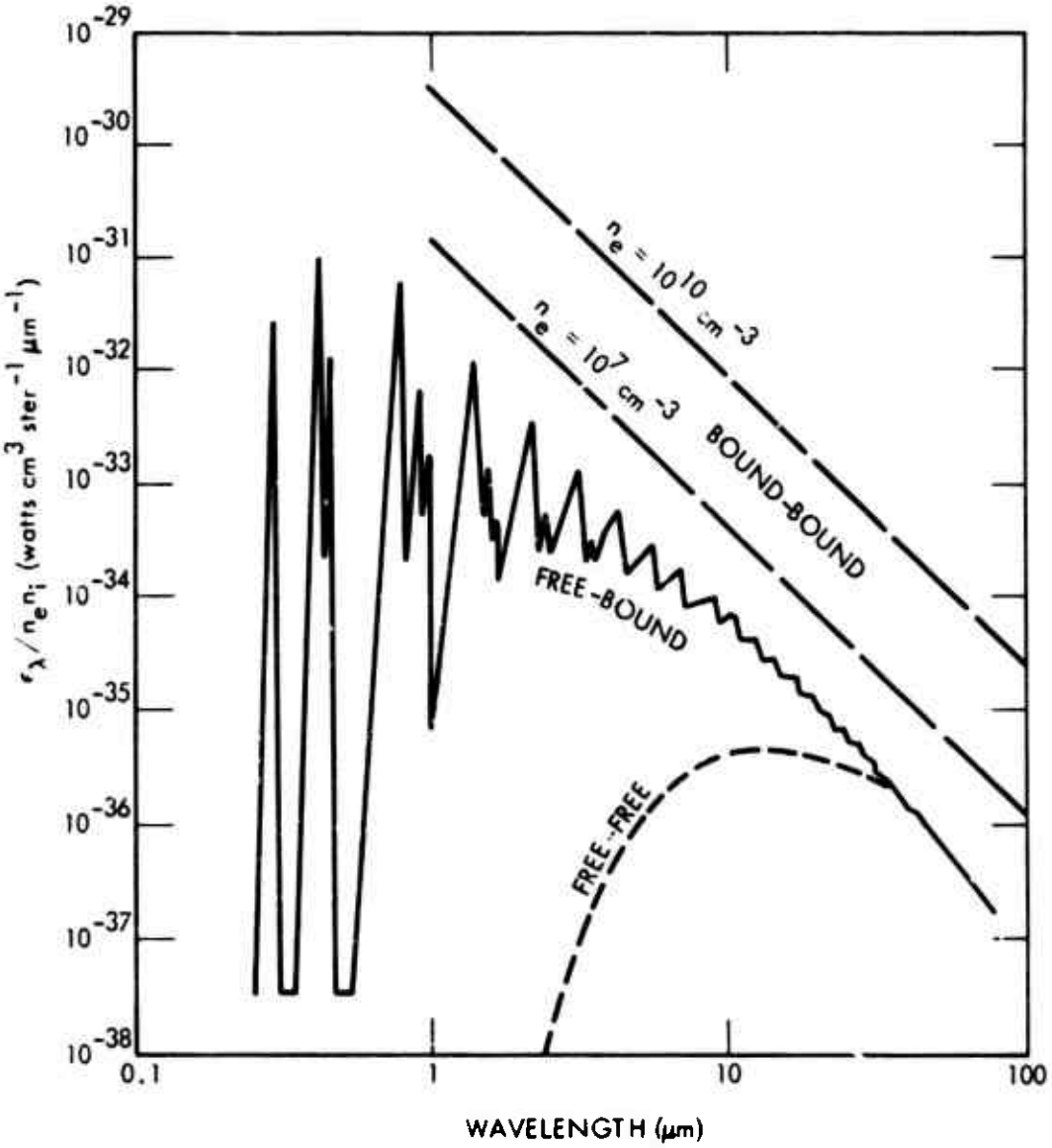

Figure 11-8. Calculated emissivities of oxygen plasma at 500 K (Reference 11-53).

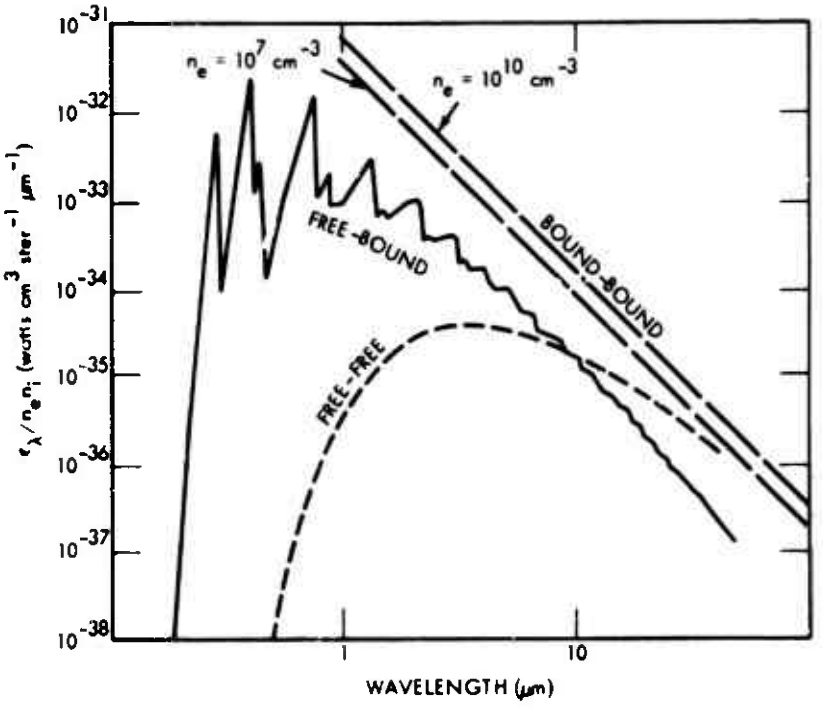

Figure 11-9. Calculated emissivities of axygen plasma at 2000 K (Reference 11-53).

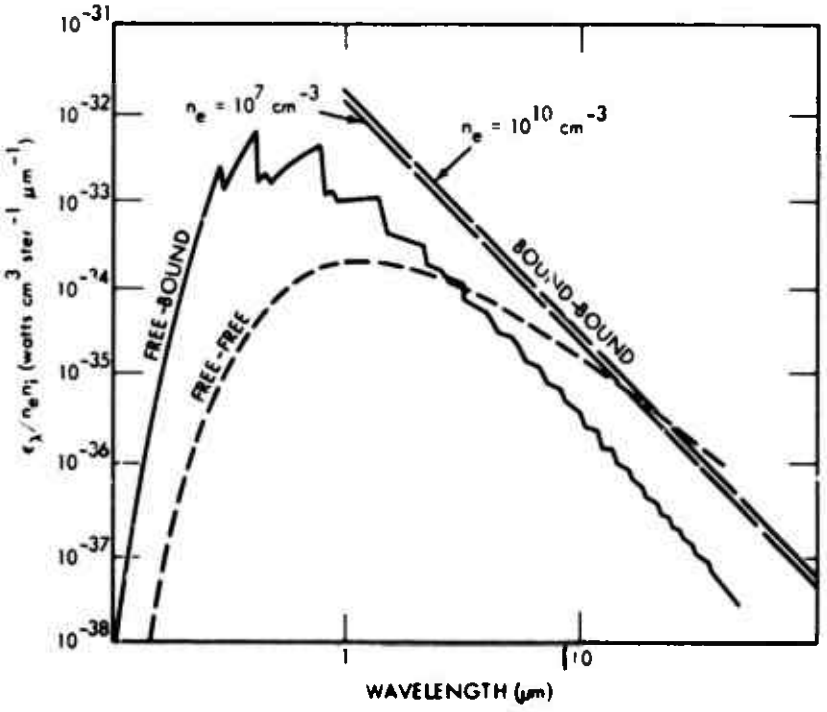

Figure 11-10. Calculated emissivities af axygen plasma at 6000 K (Reference 11-53).

emission lines in Table 12-3. Values at wavelengths less than 304 A are presented in Table 12-4. From 1250 A to the ionization threshold (1027.8 A) the spectrum is complex with several regions of low absorption (References 12-4, 12-9, 12-17, 12-25, 12-26), such as the important H Ly α window (Table 12-3). In the ionization region, Table 12-3 includes both total absorption and ionization cross-sections, and is based on several measurements (References 12-18, 12-27 through 12-30), which are in general agreement with earlier work (Reference 12-4). The cross-section curves are available in the references.

Table 12-3. Absorption and ionization cross-sections of O_2, N_2, and O at solar lines. Cross-sections in Megabarns ($10^{-18}cm^2$). Values based on data in References 12-4, 12-18, 12-27, 12-28, 12-29, 12-31, 12-36, 12-37, 12-43, and 12-47. Table prepared in collaboration with R.I. Schoen and based on Reference 12-5.

Solar Line λ (A)	Class.	O_2		N_2		O
		σ	σ_i	σ	σ_i	$\sigma = \sigma_i$
1215.7	H Ly α	0.010	0	$<6\times10^{-5}$	0	0
1206.5	Si III	15	0	~0	0	0
1175.5[a]	C III	1.3	0	-	0	0
1085.7[d]	N II	2[b]	0	-	0	0
1037.6[a]	O VI	0.78	0	$<7\times10^{-4}$	0	0
1031.9	O VI	1.04	0	$<7\times10^{-4}$	0	0
1025.7	H Ly β	1.58	.98	$<10^{-3}$	0	e
991.6[a]	N III	1.75	1.21	1.9[b,c]	0	0
989.8[a]	N III	1.4	0.95[b,c]	1.1[c]	0	e
977.0	C III	4.0	2.5	0.7[c]	0	0
972.5	H Ly γ	32	25[b]	360[b,c]	0	0
949.7	H Ly	6.3	4[b]	5.2[b]	0	0
937.8	H Ly	5.0	3	10[b]	0	e
930.7	H Ly	26	17[b]	4.8[b]	0	e
904.0	C II	11	6.3[b]	6.3	0	3.0

Table 12-3. (Cont'd.)

Solar Line λ (A)	Class.	O_2		N_2		O
		σ	σ_i	σ	σ_i	$\sigma = \sigma_i$
835.3	O III	10	3.7	20[b]	0	2.6[f]
835.1	O III	10	3.7	41[b]	0	2.6
834.5	O II	11	4.0	7.5[b]	0	2.6[f]
833.7	O III	13	5.1	6[b]	0	2.6
833.3	O II	13	5	2.3	0	2.6
832.9	O III	26	10	7[b]	0	2.6[f]
832.8	O II	26	10	2.1	0	2.6
790.2	O IV	28	10[b]	22[c]	10[b,c]	2.9
790.1	O IV	28	10[b]	28[c]	11[b,c]	2.9
787.7	O IV	24	13[b]	10[c]	8[c]	2.9[f]
780.3	Ne VIII	28	11[b]	19	-	2.9
770.4	Ne VIII	18	11	15	-	7[e]
765.1	N IV	23	12[b]	67[c]	51[b,c]	3.0
760.4	O V	20	10	40	22	2.9[f]
703.8	O III	26	23	22	20	6.5
702.3	O III	24	21	24	22	6.5
686.3	N III	22	22	25[c]	24[c]	6.5[e]
685.8	N III	18	18	26[c]	25[c]	6.5
685.5	N III	18	18	25[c]	24[c]	6.5[e]
685.0	N III	26	26	25[c]	24[c]	6.5
629.7	O V	30	29	23[c]	23[c]	9.0
625.0	Mg X	25	24	24	23	9.0
610.0	Mg X	27	25	24	24	9.0
599.6	O III	28	27	23	22	9.0
584.3	He I	23	23	23	23	9.5
555.3	O IV	26	25	25	24	9.5

Table 12-3. (Cont'd.)

Solar Line λ (A)	Class.	O_2		N_2		O
		σ	σ_i	σ	σ_i	$\sigma = \sigma_i$
554.5	O IV	26	26	25	23	9.5
554.1	O IV	26	25	25	24	9.5
553.3	O IV	26	24	25	24	9.5
537.0	He I	21	21	25	24	9.3
525.8	O III	25	24	26	26	9.3
522.2	He I	21	21	24	23	9.3
508.2	O III	24	23	22	22	9.3
507.7[d] 507.4	O III	23	22	24	24	9.3
435.0	O III	21	21	24	24	9
430.2[d] 430.0 429.9	O II	18	18	21	21	9
303.8	He I	17	17	12	12	8.5

Nares:

[a] Blend af several lines observed in salar spectrum.

[b] The absorbing gas has discrete structure at this wavelength and thus the cross-section presently measureable given in the table may not be applicable. See text and references.

[c] Considerable variation among measurements.

[d] These lines not resalved in labaratary crass-sectian measurement.

[e] Possible averlap with atomic oxygen graund-state (^3P) absarption line.

[f] Possible overlap with atomic axygen metastable-state (^1D) absorption line.

Table 12-4. Absorption cross-sections[a] at wavelengths less than 304 A. Data primarily from References 12-47, 12-89, 12-90. Cross-sections in Megabarns (10^{-18} cm^2).

Wavelength[b] (A)	O_2	N_2	O
247.2	12.3	9.8	6
209.3	9.0	6.5	4
100	1.9	.84	0.8
68.0	.9	.50	.2
44.6	.31	.18	.1
13.4	.29	.089	.14[c]
9.9	.14	.042	.071[c]

Notes:

a These cross-sections are assumed to be equal to the ionization cross-section at least to 100 A, although there are no yield measurements.

b There are a number of solar lines in this region, but there have been few measurements, and also the cross-section curve appears to be relatively smooth. The wavelengths used should allow a reasonable estimate to be made.

c This value is one-half the O_2 cross-section.

The dissociative ionization process giving O^+ and O begins at 662 A, and the yield appears to be less than 10 percent of the total ionization yield in the region down to about 450 A, with a conventional magnetic mass spectrometer (Reference 12-31). However, excess kinetic energy has been found in the product ions, and a more recent estimate is 15 percent dissociative ionization at the 584 A line (Reference 12-32). The cross-sections for excitation to various specific molecular ions over a range of wavelengths (Reference 12-33) are given in Figures 12-5 and 12-6. These were obtained by energy analysis of the emitted electrons.

Appreciable quantities of the metastable oxygen $O_2(a\,^1\Delta_g)$ molecule appear to be present in the upper atmosphere (References 12-34, 12-35). It is conceivable that absorption by this molecule may be

$2p^3\ ^2P^o$. These lines have been classified and measured in absorption (Reference 12-36), which enables the previously unknown autoionized lines to be observed. The lower members of these series are shown in Figures 12-8 and 12-9, with the unautoionized levels indicated by an asterisk. Accidental line absorption (References 12-48, 12-50) has led to cross-section measurements that are larger than nearby points, as shown by the dashed lines beneath some points in Figures 12-8 and 12-9.

There has been a theoretical calculation of some autoionized line profiles (Reference 12-51). The published calculations used a bandwidth corresponding to 1 A. Since the measurements used atomic lines, this bandwidth is considerably too large to use in a meaningful comparison with experimental values. Further calculations using a 0.1 A bandwidth (Reference 12-52) are shown in Figures 12-8 and 12-9. These profiles and maxima are in much better agreement with the available cross-sections and with estimates of absorption line maxima (Reference 12-53). Some maxima are not shown because the calculated points were too widely spaced in wavelength.

Both the $2p^4\ ^1D_2$ and $2p^4\ ^1S_o$ metastable states of atomic oxygen are known to be present in the atmosphere. Measurements of absorption series of these metastables have been reported (Reference 12-37). There also exist calculations of their ionization cross-sections (Reference 12-46) and a review of $O(^1D)$ formation and reactions (Reference 12-54).

It is possible that atmospheric spectrophotometric measurements may be influenced by the accidental overlap of a solar emission line and an atomic oxygen line (Reference 12-53). An abridged version of the possible solar lines involved is given in Table 12-5.

For a number of atmospheric problems, the cross-sections for ionization between specific electronic states of the atom and the ion are required. These are given for all $2p^4 \rightarrow 2p^3$ transitions in Figure 12-11 (Reference 12-55), which is based on an interpolation formula developed following close-coupling calculations (Reference 12-56). This formula does not include the autoionization structure apparent in Figures 12-8 and 12-9, which is based on experiment and on more detailed calculations. Therefore, Figures 12-8 through 12-10 are more useful for total attenuation calculations and Figure 12-11 is necessary to calculate the products.

Table 12-5. Atomic oxygen lines which moy absorb solor lines. Atomic oxygen resononce lines (1302, 1305, 1306 A) not included. References 12-36, 12-37, 12-53 give detoils.

Solor Line (A)	O I Line (A)	Clossificotion	Remorks
1025.7	1025.7	$^3P_2 - 3d\,^3D^o$	a
989.8	990.13	$^3P_1 - 3s'\,^3D^o$	
937.8	937.84	$^3P_2 - 7s'\,^3S^o$	
930.7	930.89	$^3P_1 - 7d\,^3D^o$	
835.3	835.44	$^1D_2 - 10d'\,^1F^o,\ ^1D^o$	
834.5	834.34	$^1D_2 - 12s'\,^1D^o$	
832.9	833.10	$^1D_2 - 12d'\,^1F^o,\ ^1D^o$	
787.7	788.18	$^1D_2 - 5s''\,^1P^o$	b
770.4	770.35	$^3P_1 - 4d'\,^3P_2{}^o$	
761.1	761.26	$^1D_2 - 6d''\,^1F^o,\ ^1D^o$	b
686.3	686.28	$^3P_1 - 5d''\,^3P^o,\ ^3D^o$	b,c
685.5	685.54	$^3P_2 - 5d''\,^3P^o\,^3D^o$	b,c

Notes:

a Solor line known to be brood.

b Atomic oxygen line broodened by outoionizotion.

c These lines known to overlap. See References 12-25 ond 12-27.

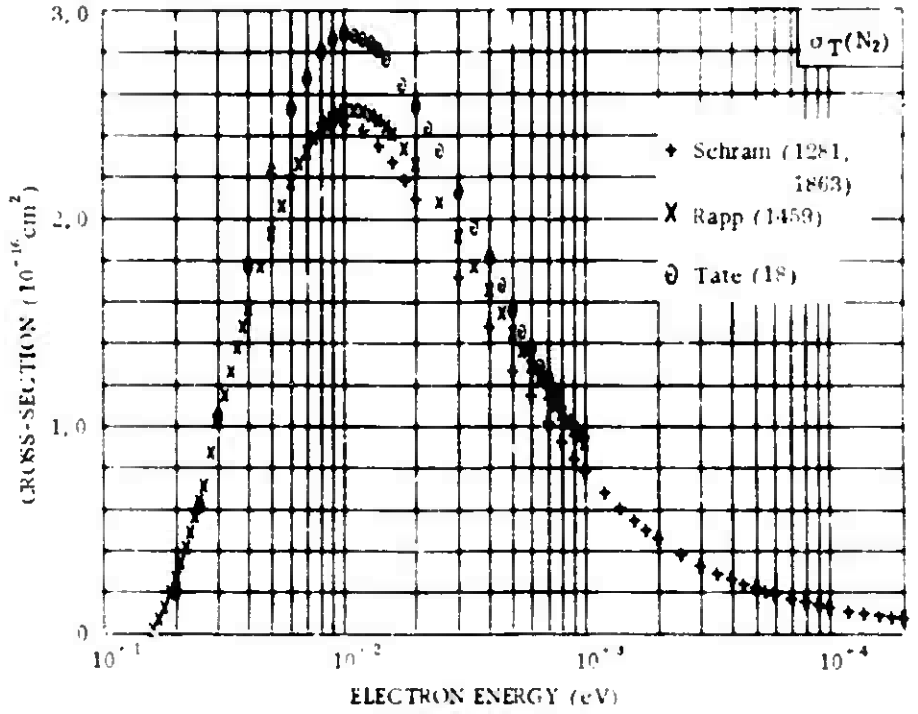

Figure 14-29.

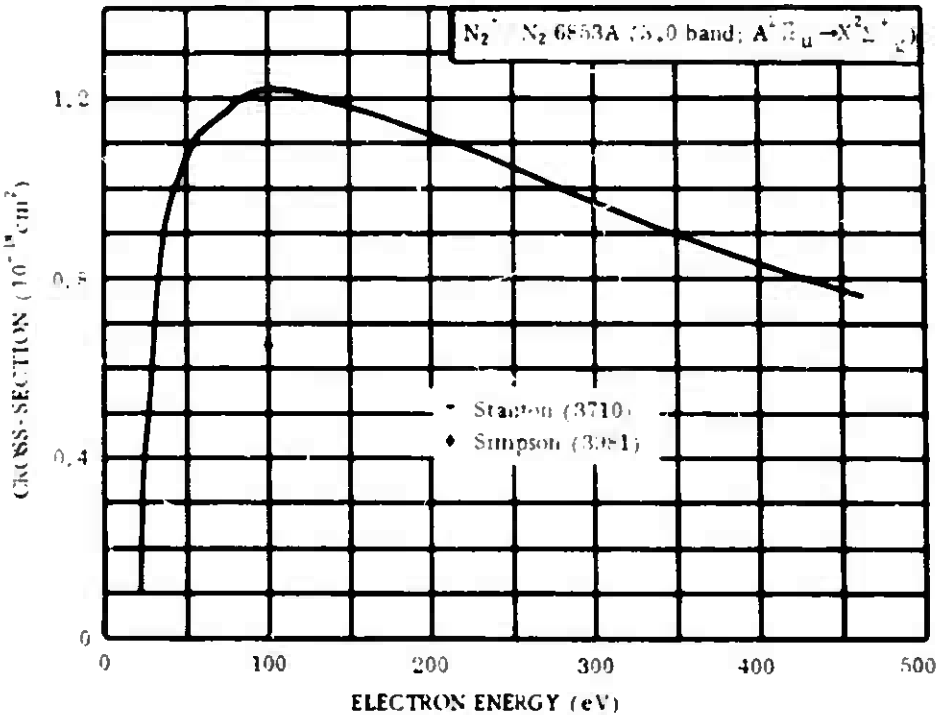

Figure 14-30.

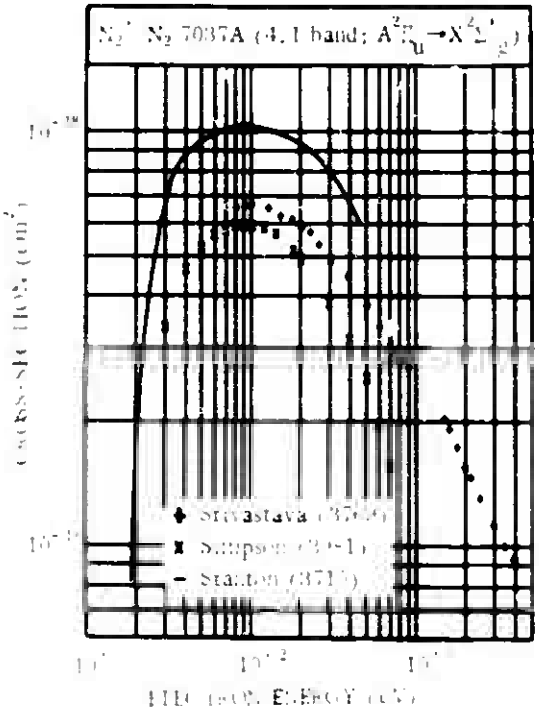

Figure 14-31.

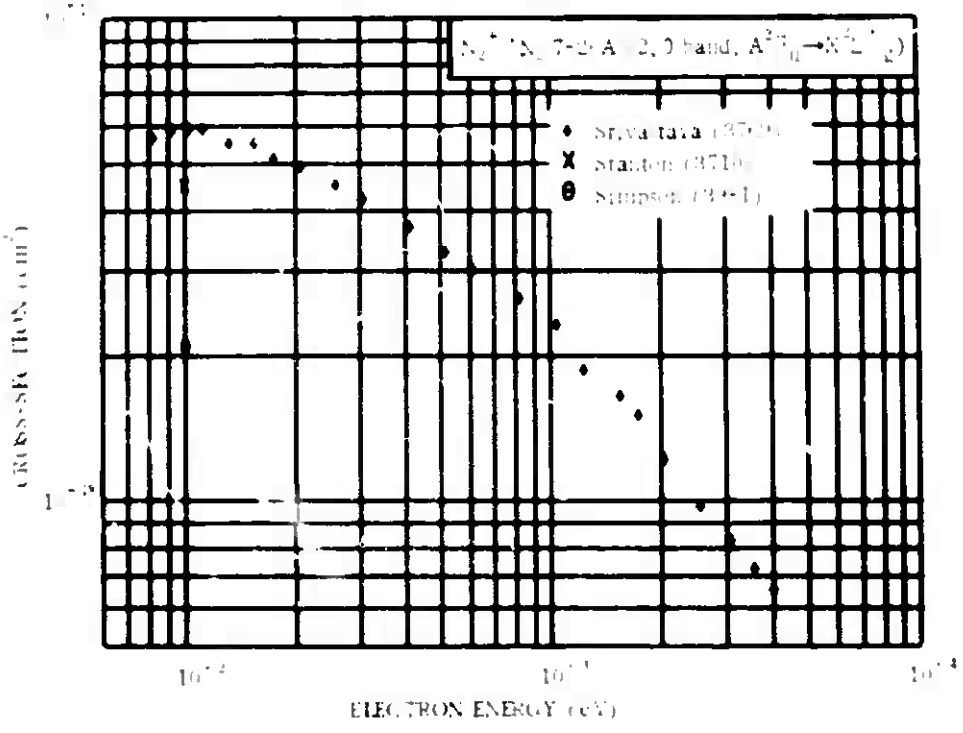

Figure 14-32.

Table 14-1. Effective line excitation cross-sections of the Meinel bands of N_2^+.

N_2^+/N_2

Wovelength[1] (A)	v', v''	E (eV)	$\sigma(10^{-19}\ cm^2)$
6106	4,0	100.	$\begin{cases} 2.4^a \\ 1.4^b \end{cases}$
6268	5,1	100.	2.7^a
7240	5,2	100.	$\begin{cases} 0.6^a \\ 1.3^b \end{cases}$
9145	1,0	100.	$110.^a$
9431	2,1	100.	$58.^a$
11036	0,0	100.	$80.^a$

Notes:

[1] The electronic transition for this system is $A^2\Pi_u - X^2\Sigma_g^+$.

[a] The data were taken from Stanton (3710).

[b] The data were taken from Simpson (3981).

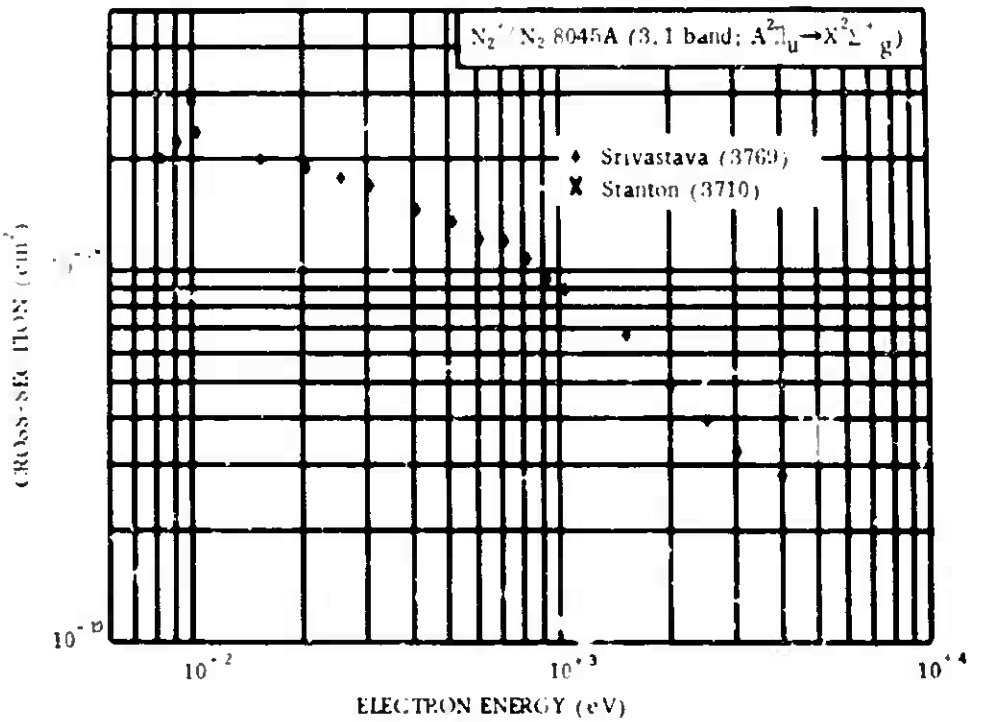

Figure 14-33.

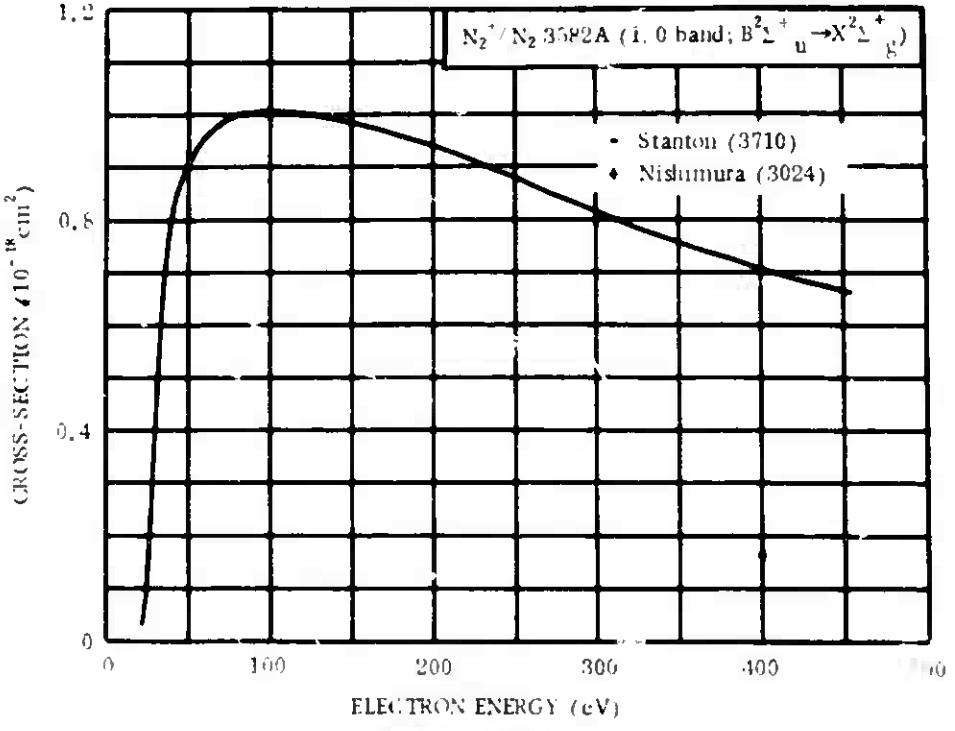

Figure 14-34.

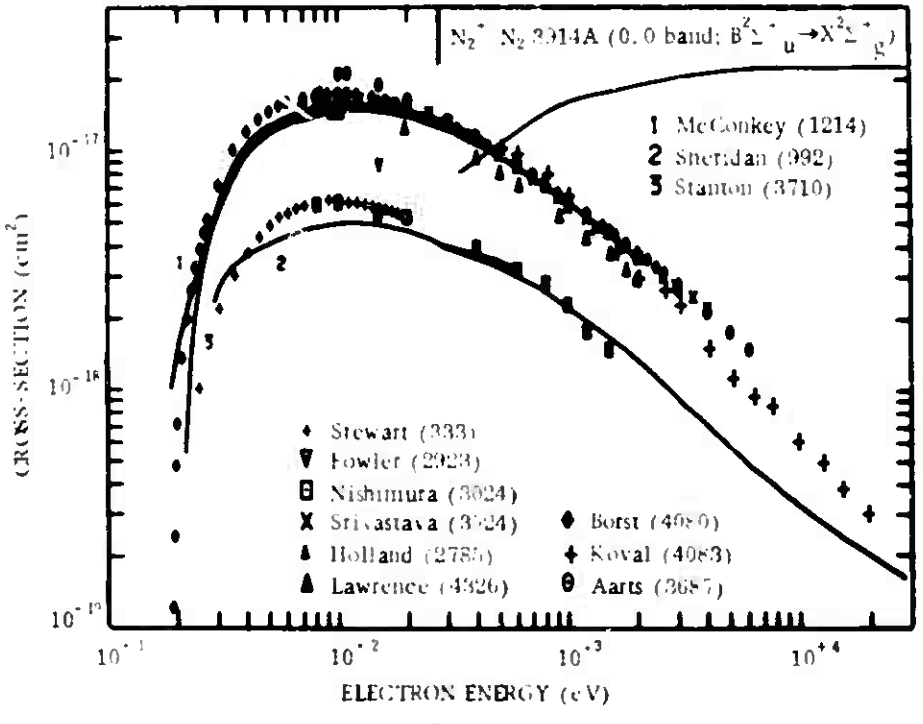

Figure 14-35.

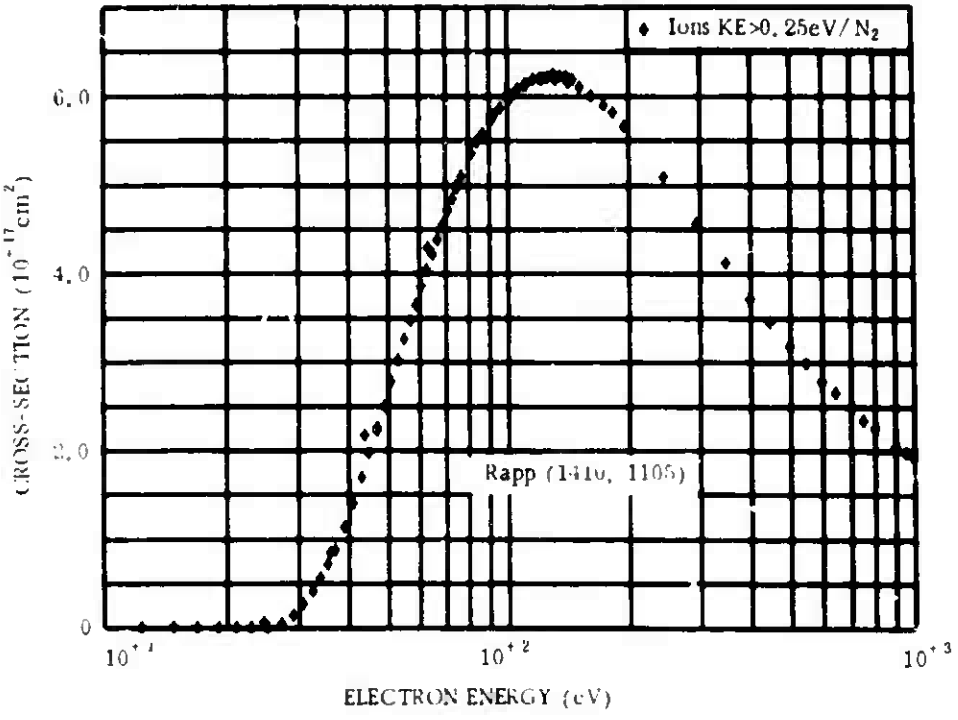

Figure 14-38.

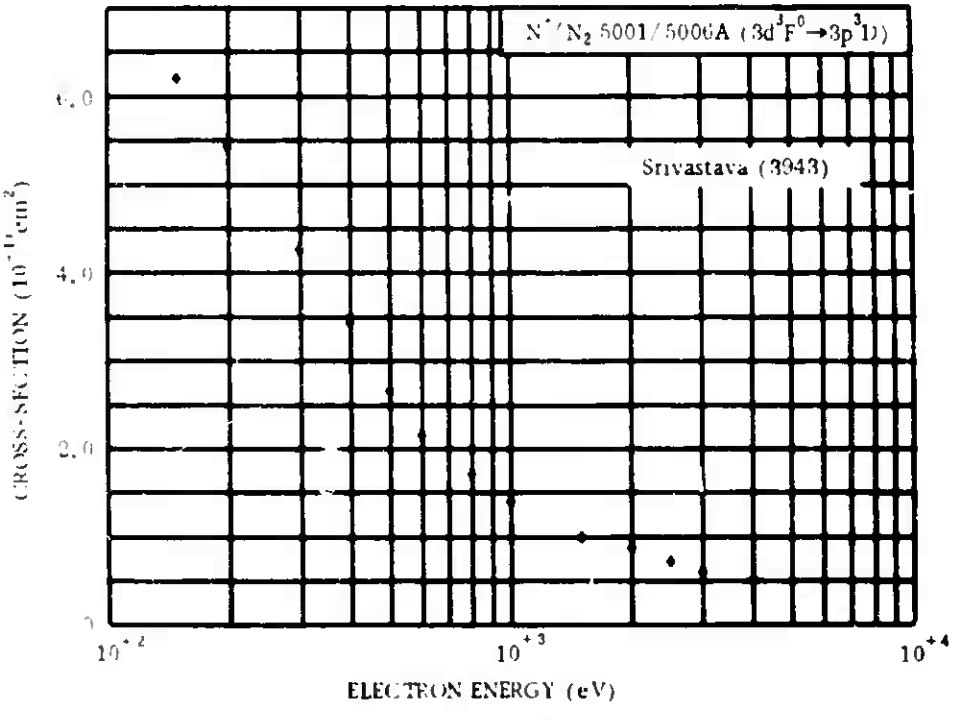

Figure 14-39.

Table 14-3. Effective dissaciative ionization cross-sectians of N_2 .

N^+/N_2

Wavelength (A)	Transition	E (eV)	$\sigma(10^{-18}\ cm^2)$ [1]
623.9	$3s'\ ^5P \rightarrow 2p'\ ^5S$	100.	0.23
645.6	$2p'\ ^3S \rightarrow 2p\ ^3P$	100.	0.25
671.4	$2s\ ^3P \rightarrow 2p\ ^3P$	100.	4.5
746.4	$3s'P \rightarrow 2p\ ^1D$	100.	3.2
746.4	$2p'\ ^1P \rightarrow 2p\ ^1S$	100.	3.2
775.1	$2p'\ ^1D \rightarrow 2p\ ^1D$	100.	2.3
918	$2p'\ ^3P \rightarrow 2p\ ^3P$	100.	11.9
1084.4	$2p'\ ^3D \rightarrow 2p\ ^3P$	100.	20.4
5667	$3p\ ^3D_2 \rightarrow 3s\ ^3P_1$	500.	0.0886
5680	$3p\ ^3D_3 \rightarrow 3s\ ^3P_2$	500.	0.231

Nate:

[1] Cross-sections at 100 eV were measured by Sroka (3833); cross-sections at 500 eV were measured by Srivastava (3943).

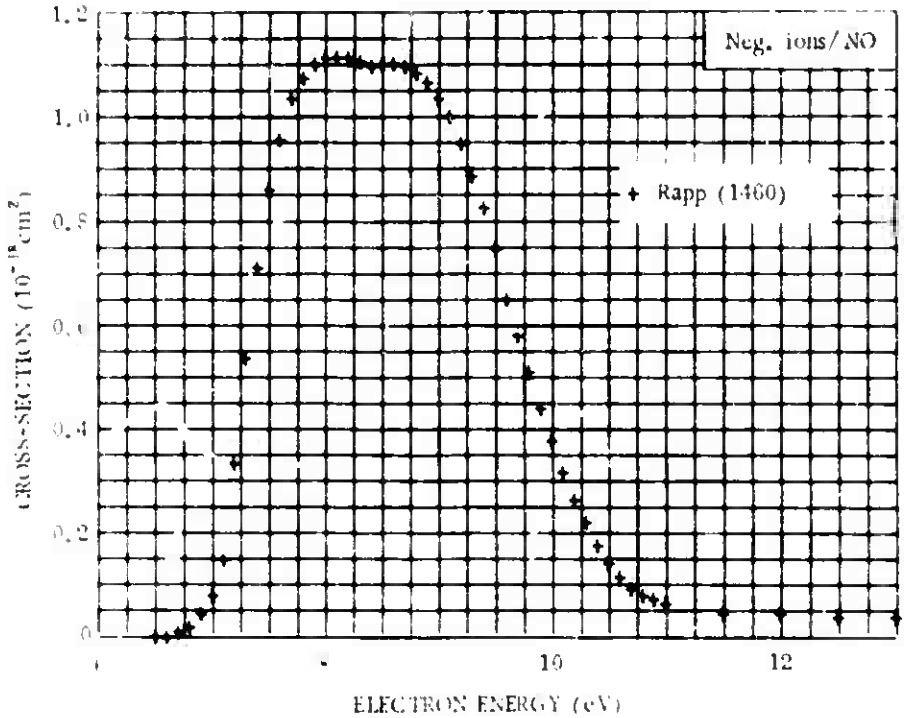

Figure 14-44.

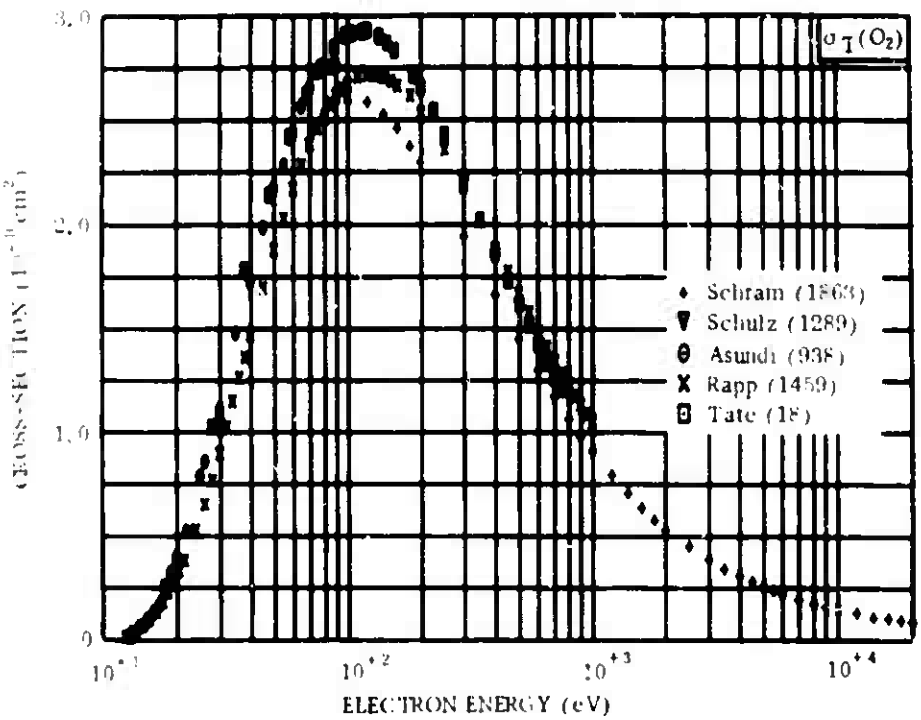

Figure 14-45.

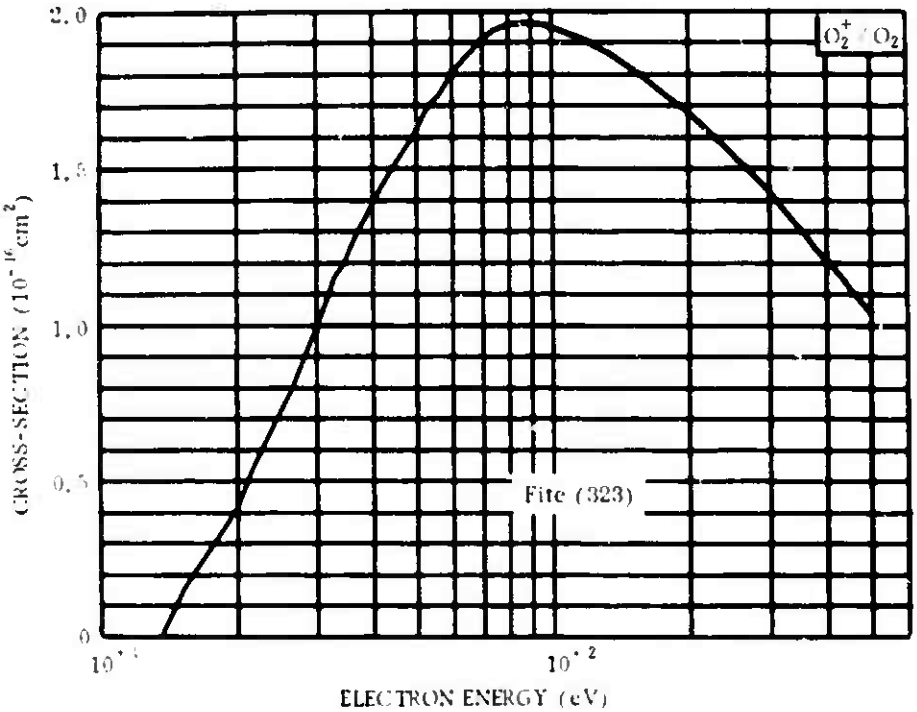

Figure 14-46.

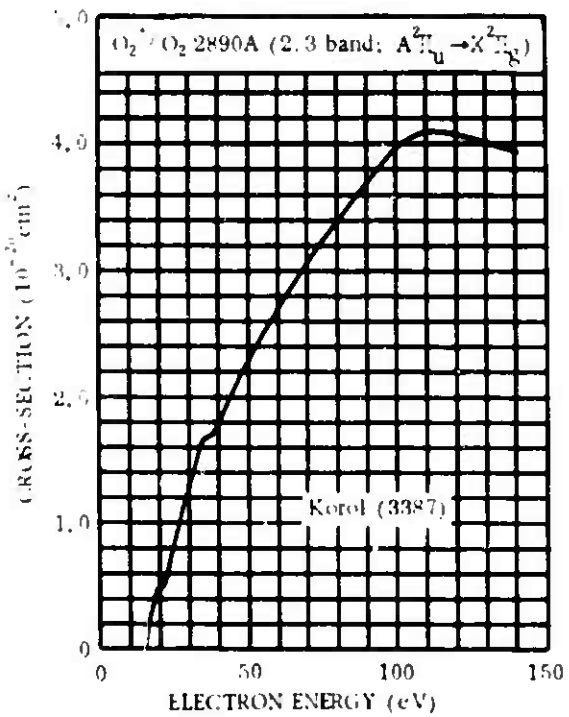

Figure 14-47.

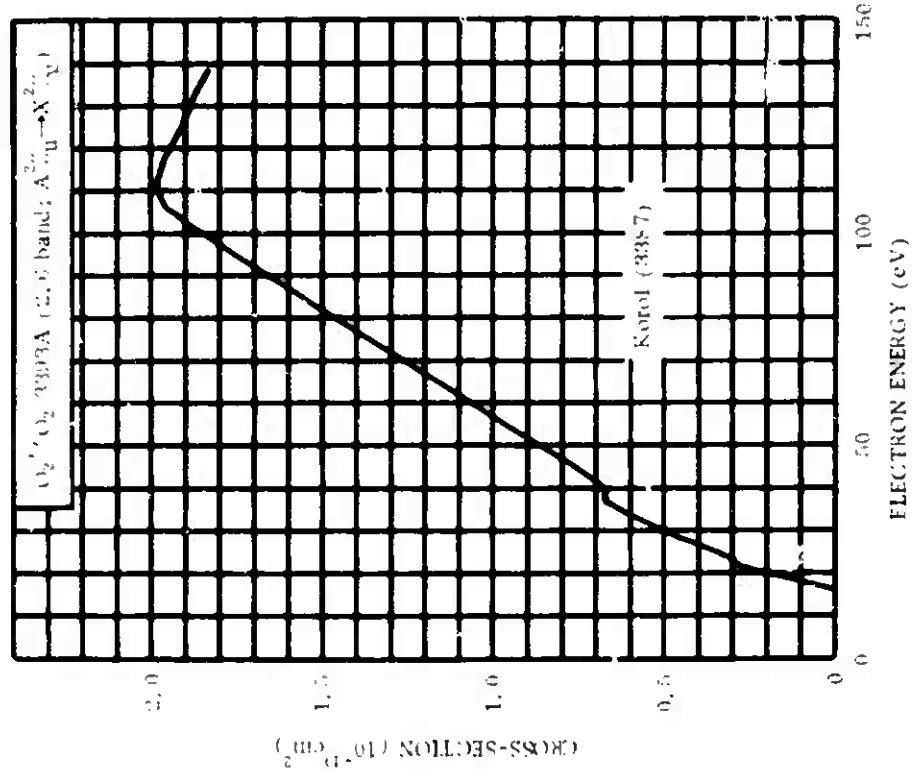

Figure 14-49.

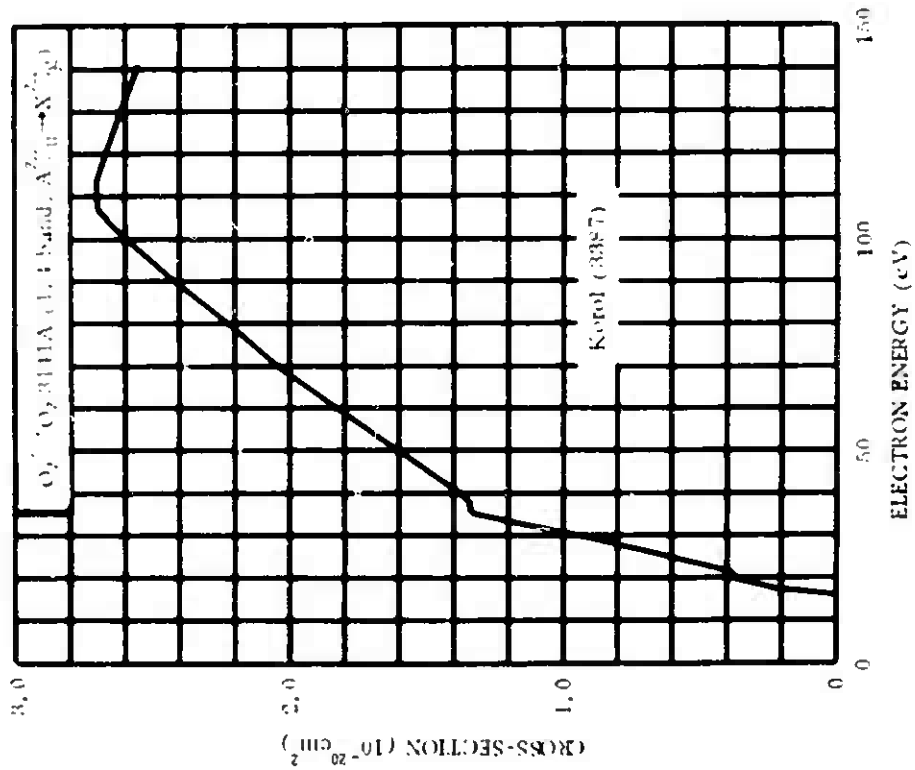

Figure 14-48.

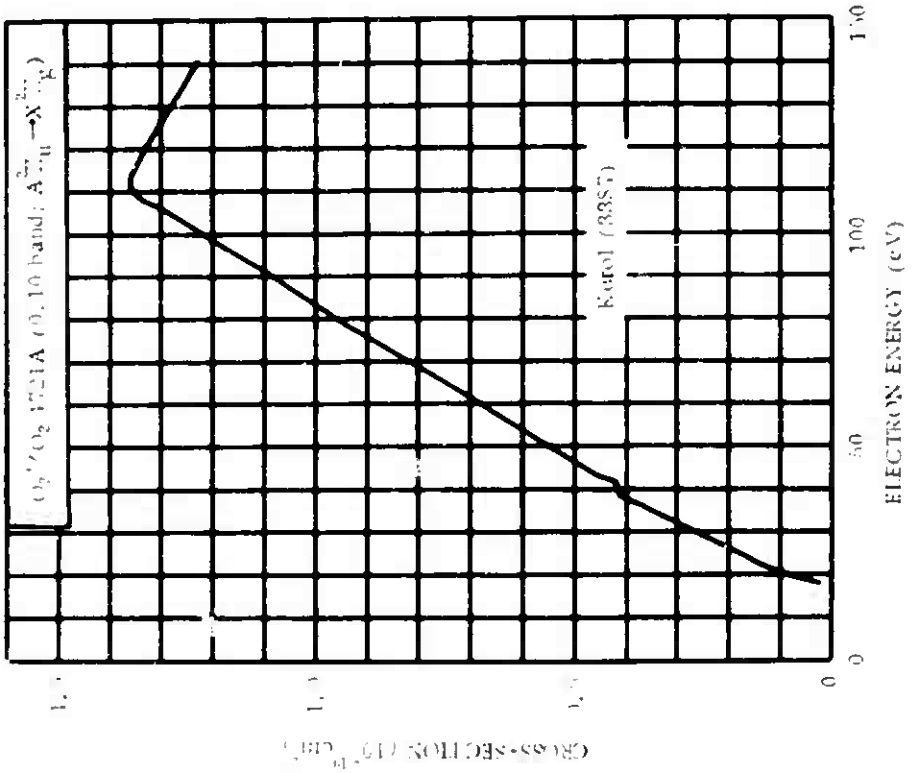

Figure 14-51.

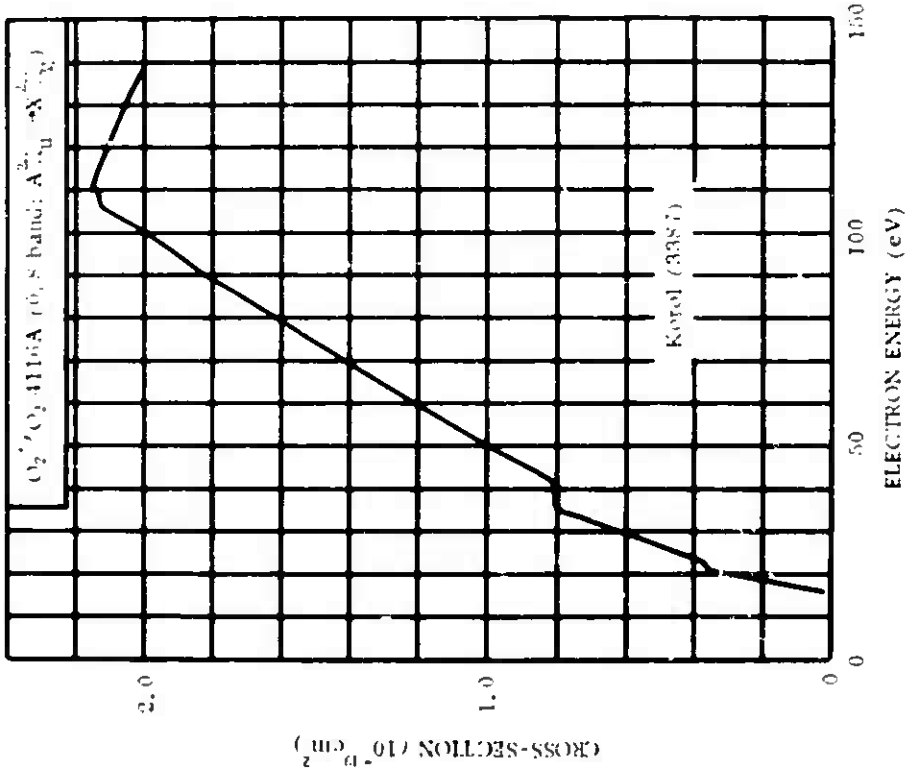

Figure 14-50.

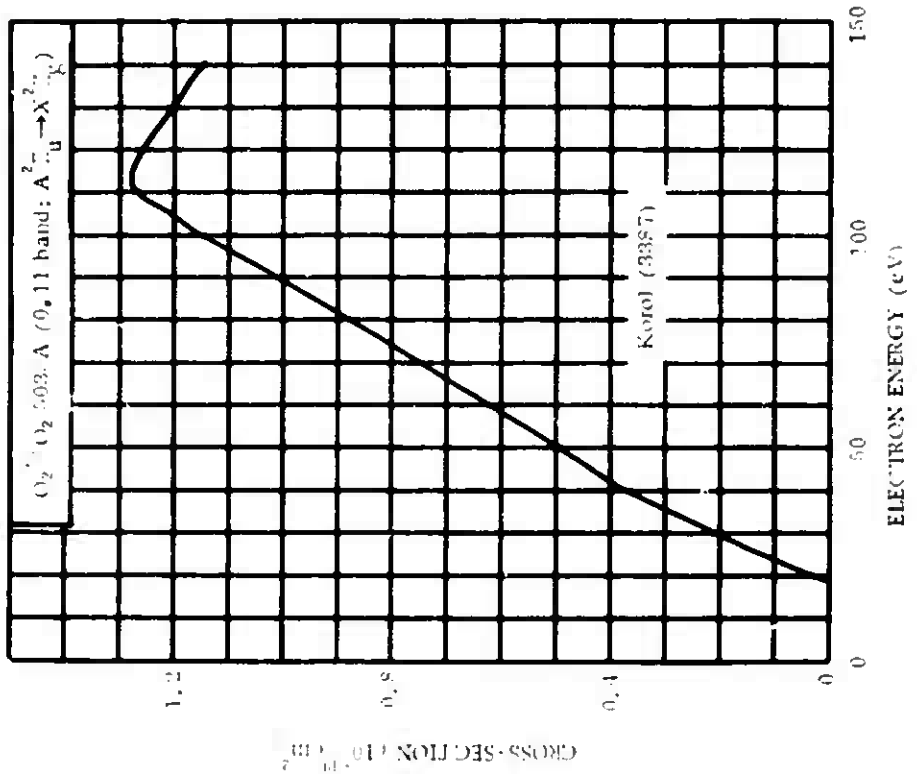

Figure 14-53.

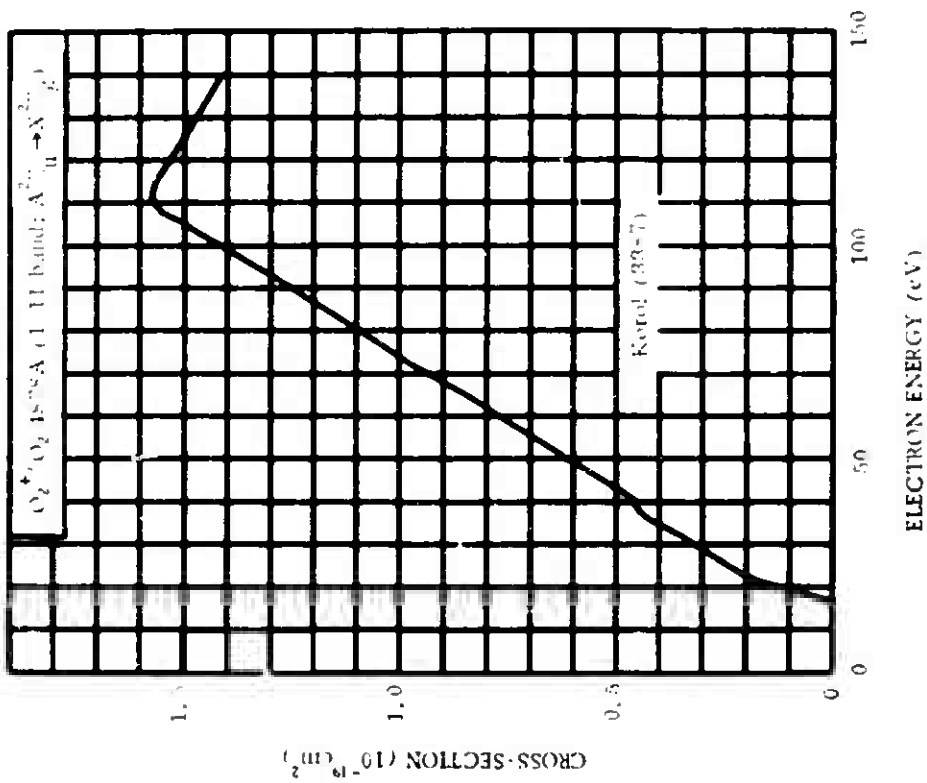

Figure 14-52.

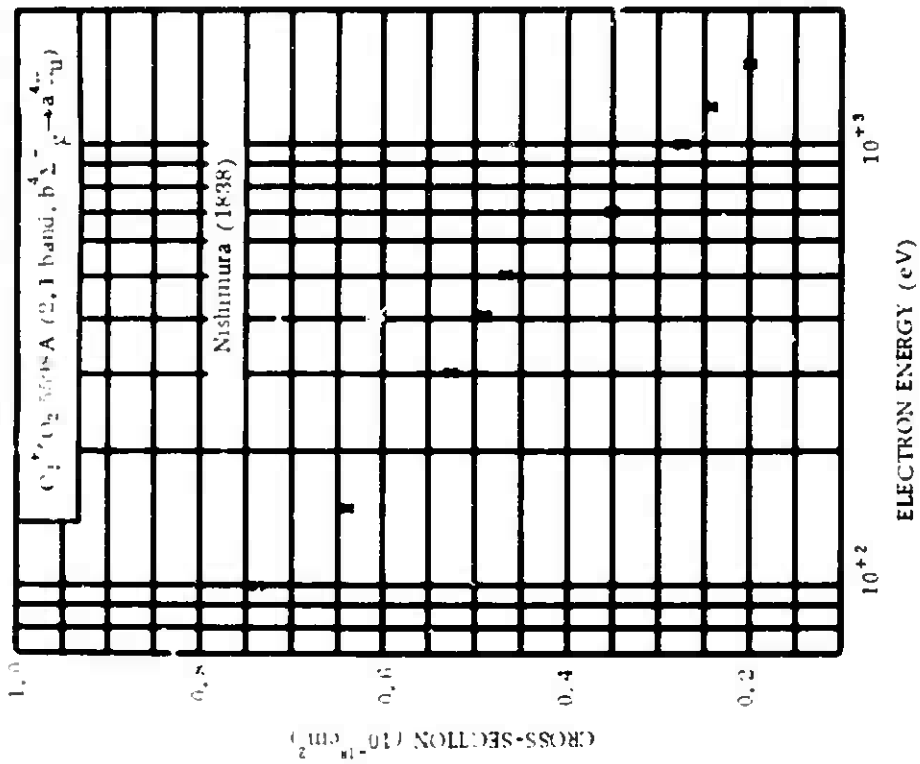

Figure 14-55.

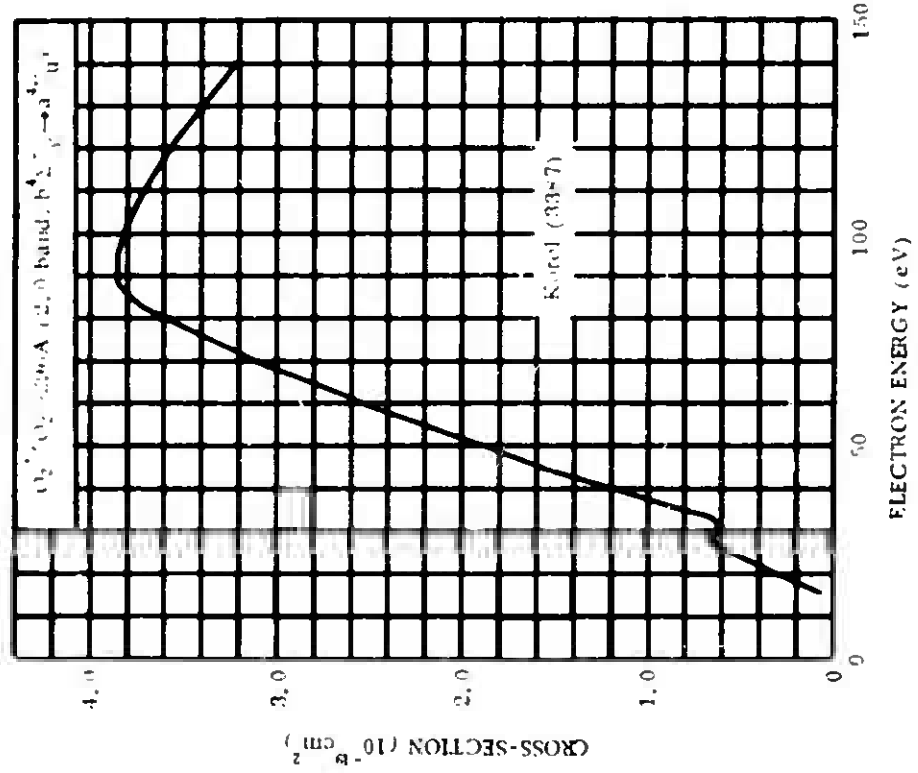

Figure 14-54.

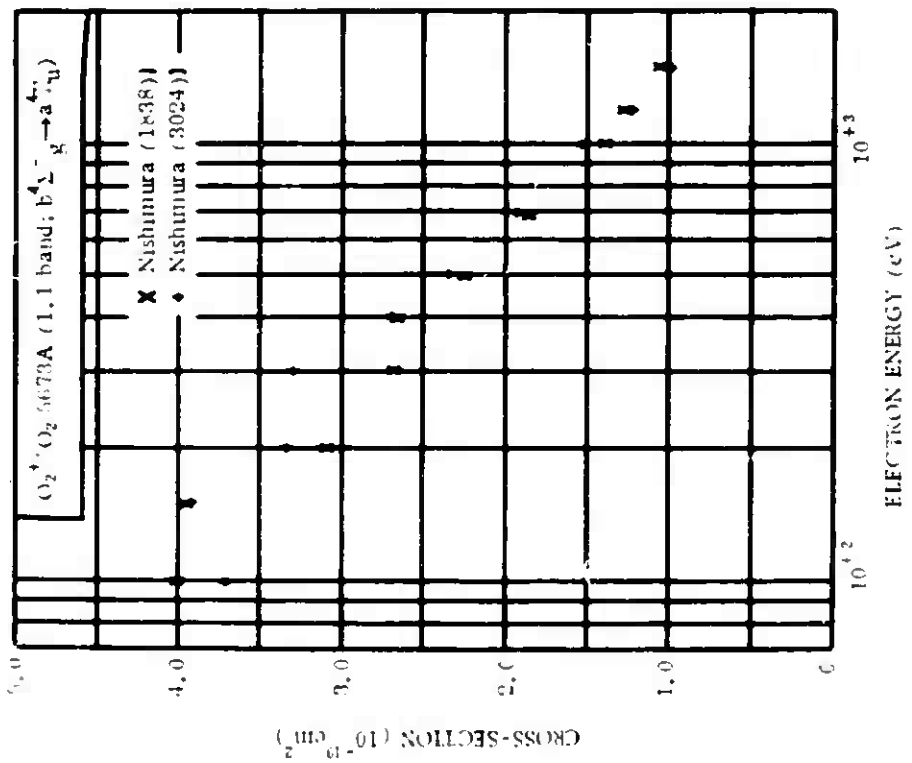

Figure 14-57.

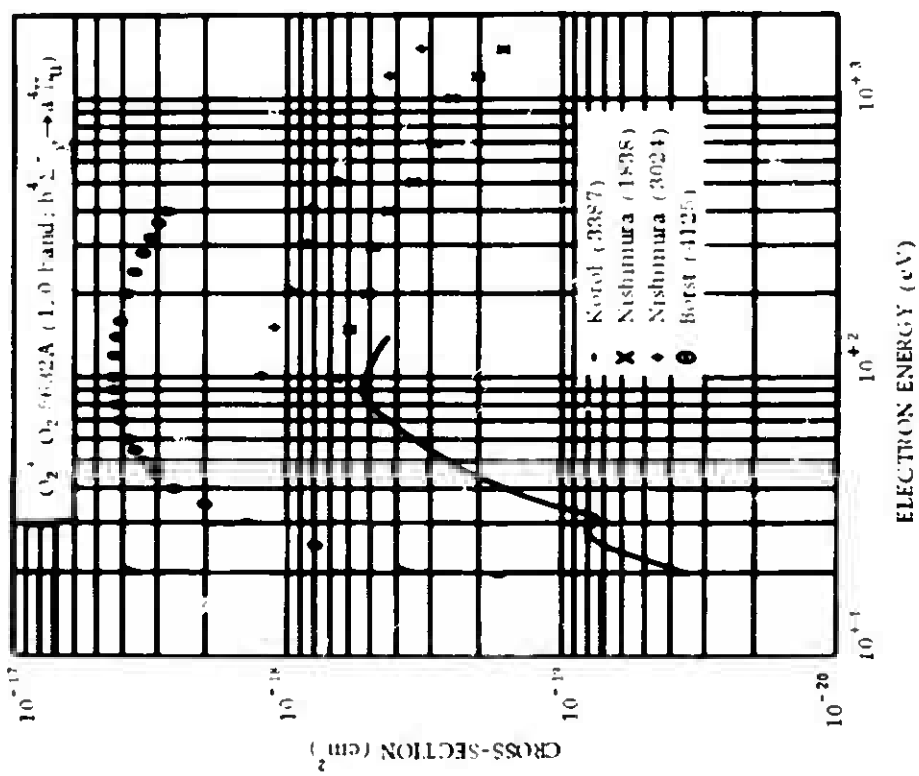

Figure 14-56.

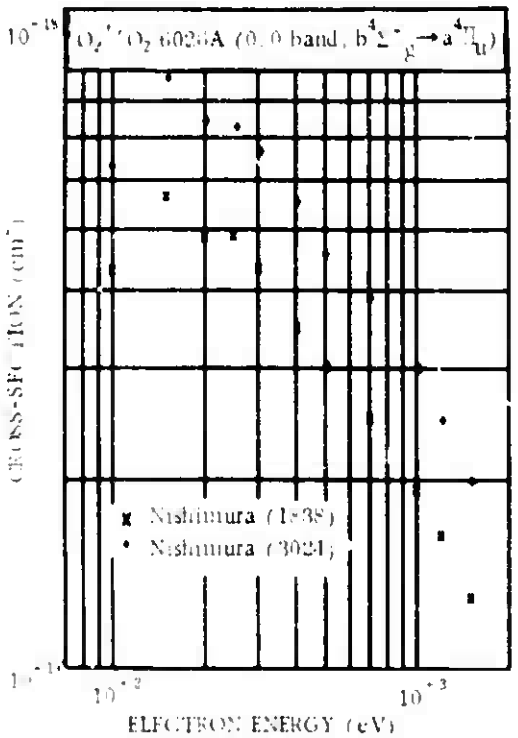

Figure 14-58.

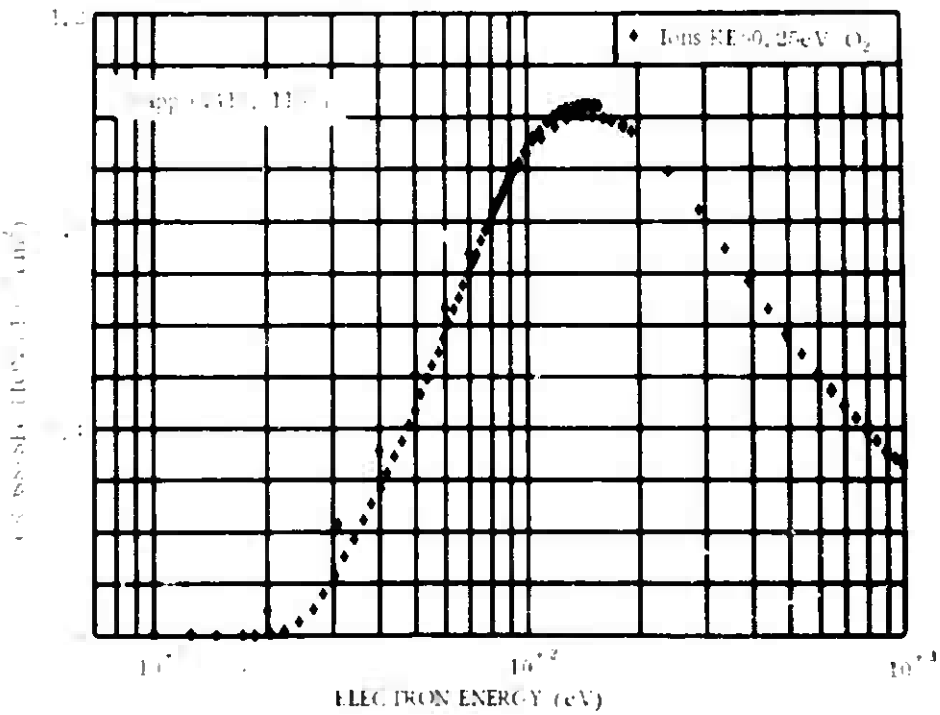

Figure 14-59.

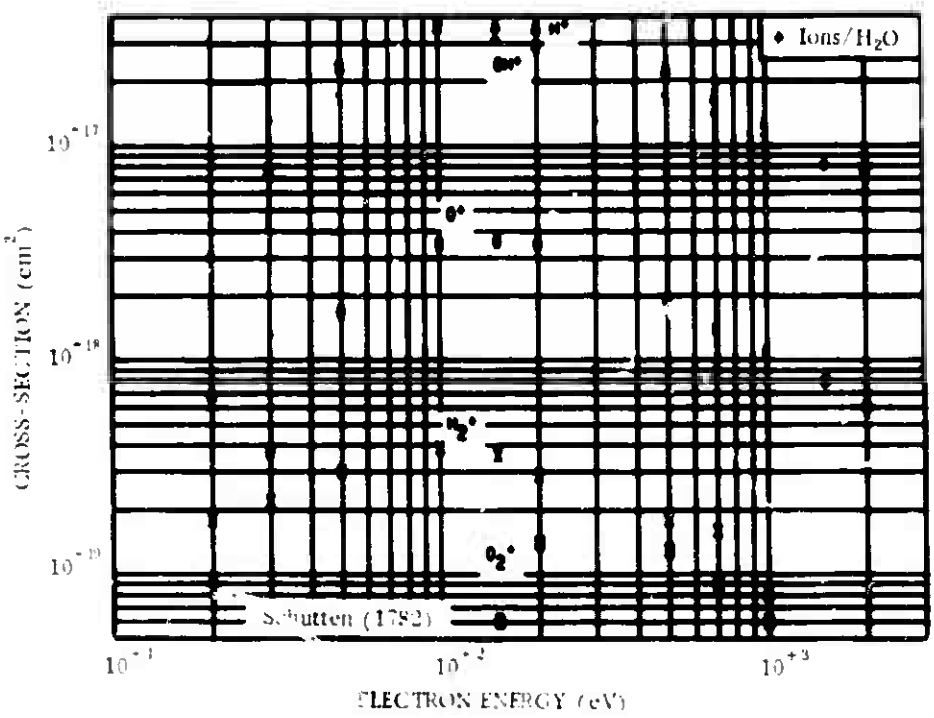

Figure 14-64.

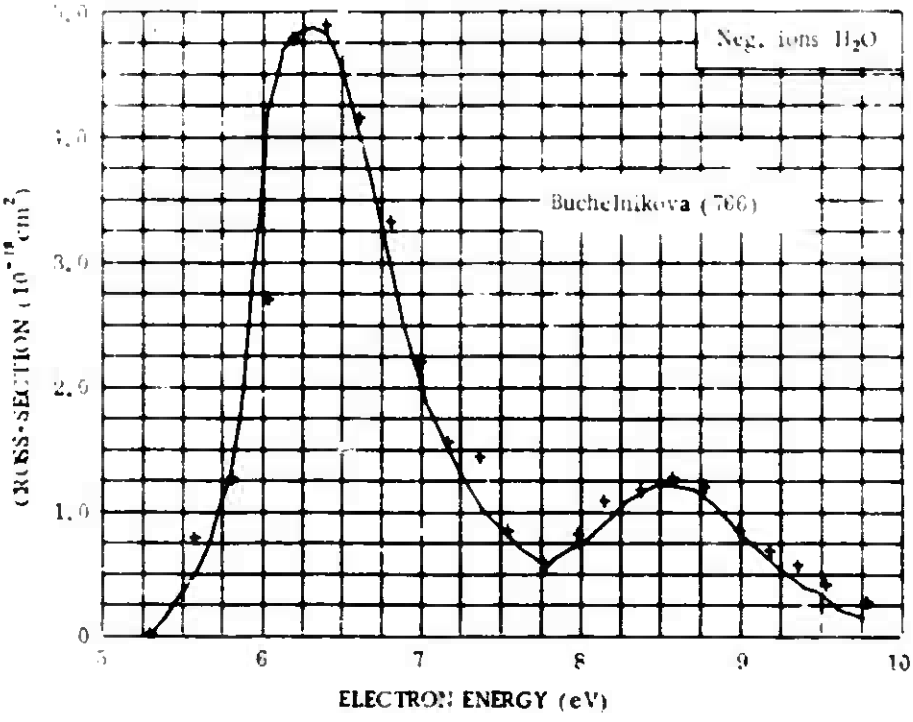

Figure 14-65.

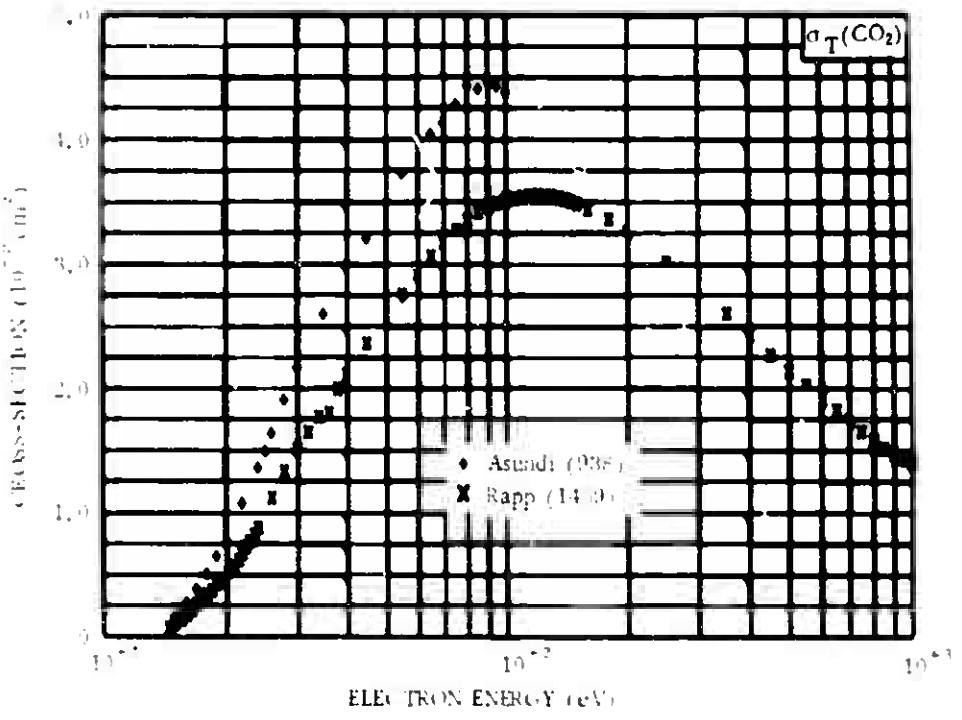

Figure 14-66.

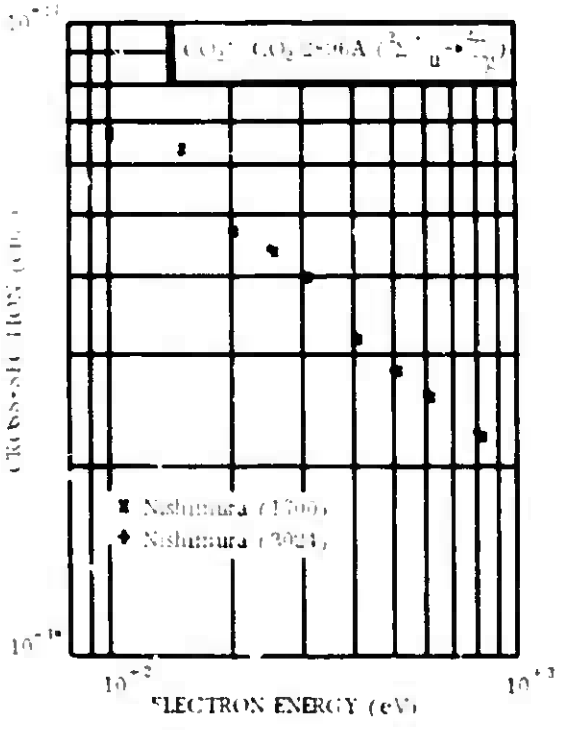

Figure 14-67.

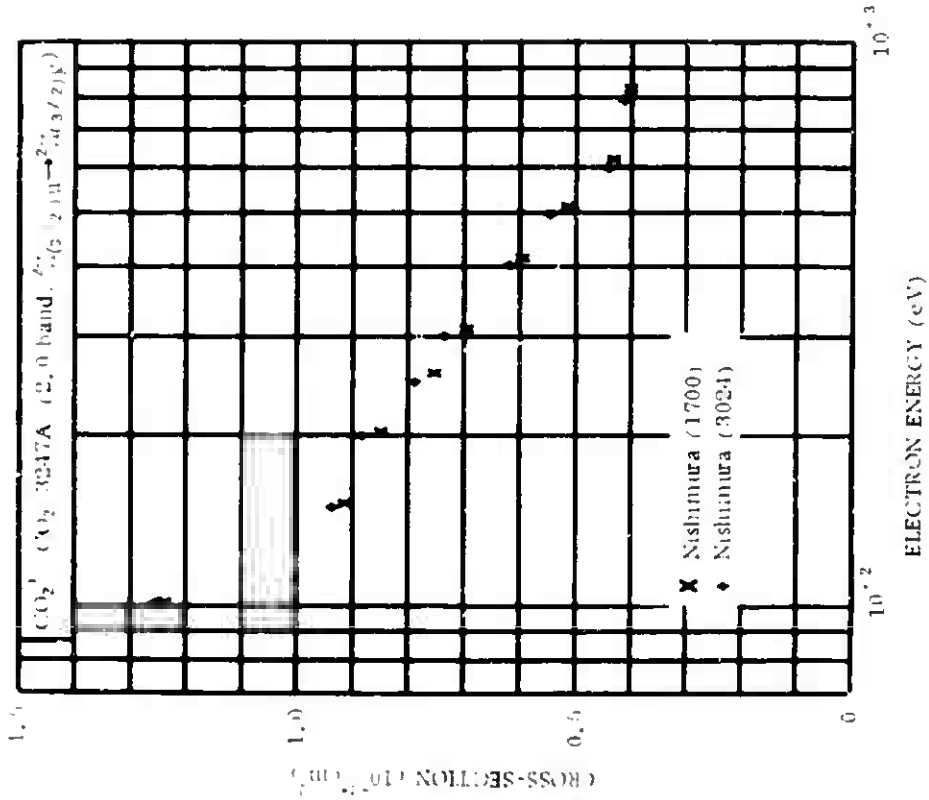

Figure 14-69.

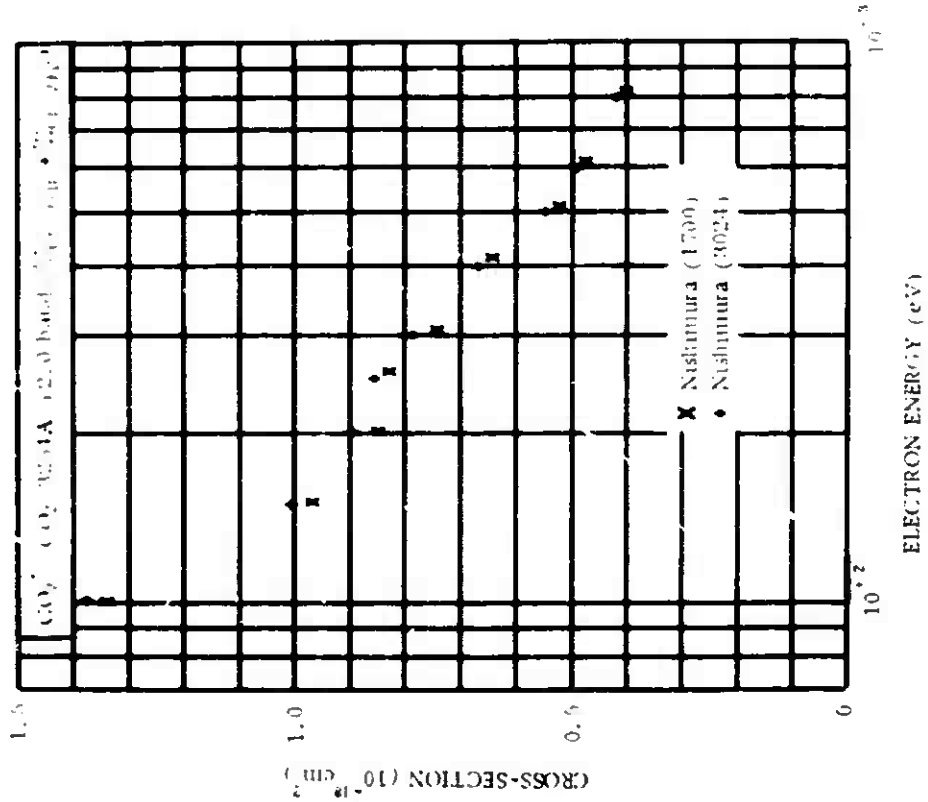

Figure 14-68.

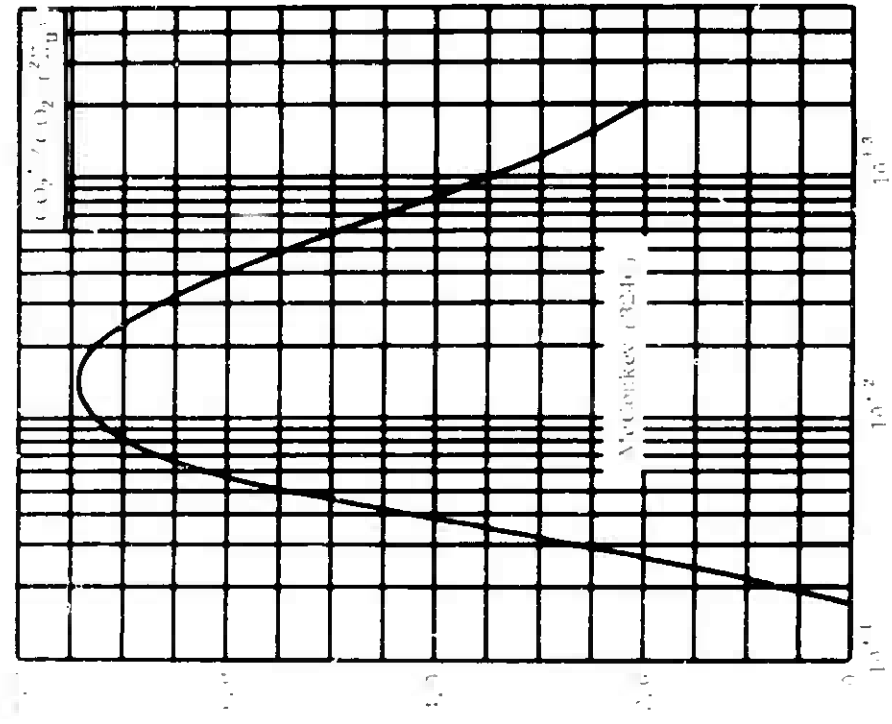

Figure 14-71.

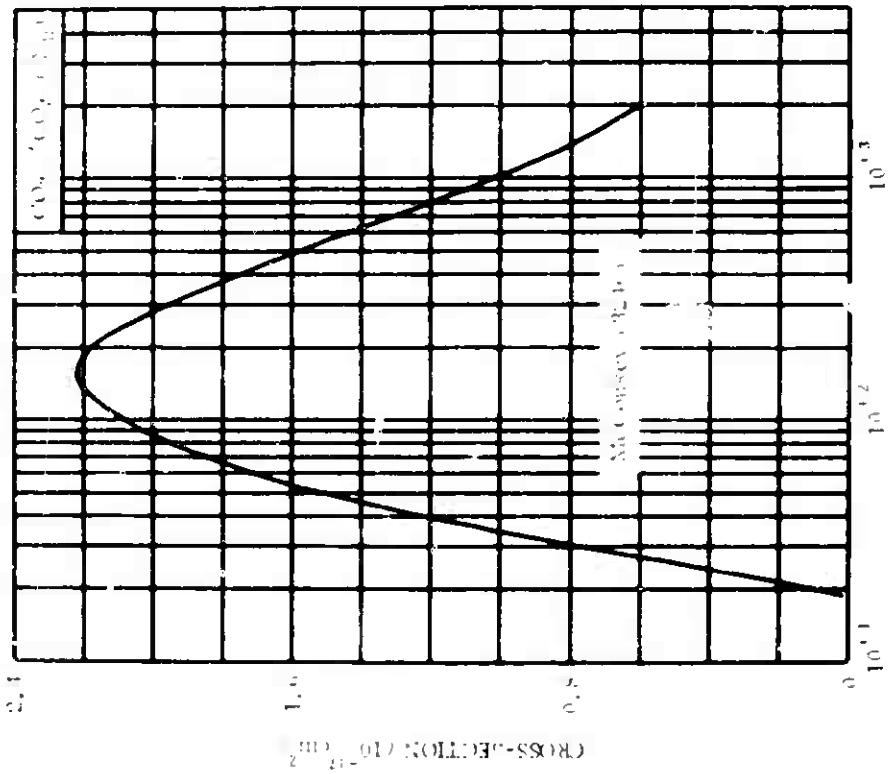

Figure 14-70.

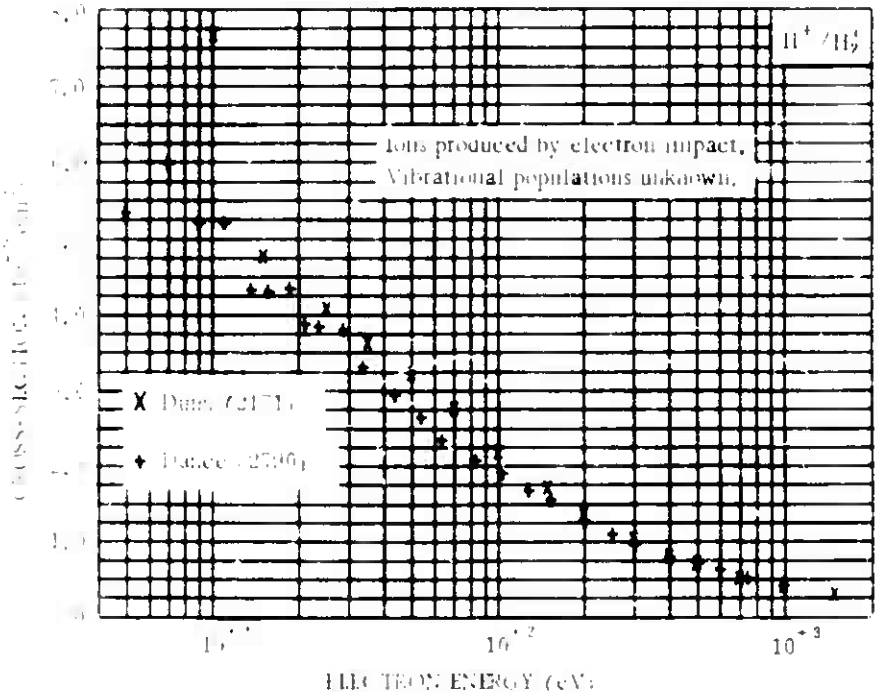

Figure 14-89.

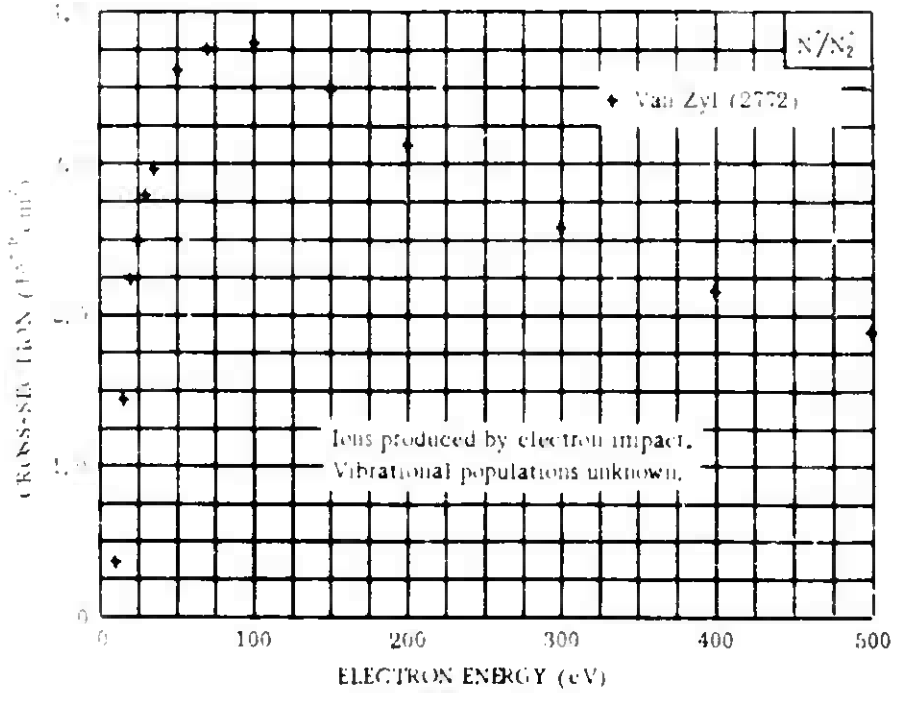

Figure 14-90.

BIBLIOGRAPHY*

(17) Vaughan, A. L., Phys. Rev. 38, 1687 (1931).

(18) Tate, J. T., and P. T. Smith, Phys. Rev. 39, 270 (1932).

(225) Smith, P. T., Phys. Rev. 36, 1293 (1930).

(261) Harrison, M. F. A., K. T. Dolder, and P. C. Thonemann, Proc. Phys. Soc. 82, 368 (1963).

(320) Fite, W. L., and R. T. Brackmann, Phys. Rev. 112, 1141 (1958).

(323) Fite, W. L., and R. T. Brackmann, Phys. Rev. 113, 815 (1959).

(324)[b] Schulz, G. J., Phys. Rev. 113, 816 (1959).

(333) Stewart, D. T., Proc. Phys. Soc. A69, 437 (1956).

(357) Tozer, B. A., and J. D. Craggs, J. Elec. Control 8, 103 (1960).

(389) Glupe, G., and W. Mehlhorn, Phys. Letts. 25A, 274 (1967).

(651)[a] Haas, R., Z. Physik 148, 177 (1957).

(743) Asundi, R. K., and M. V. Kurepa, J. Elec. Control 15, 41 (1963).

(760)[b] Buchelnikova, N. S., Sov. Phys. - JETP 8, 783 (1959).

(938)[b] Asundi, R. K., J. D. Craggs, and M. V. Kurepa, Proc. Phys. Soc. 82, 967 (1963).

---

* The citation number listed to the left of each entry refers to its JILA Information Center citation number, and should be used in any pertinent correspondence with JILA or with the authors of this chapter.

[a] Vibrational and rotational excitation.

[b] Dissociation processes.

16. CHARGED-PARTICLE RECOMBINATION PROCESSES

Monfred A. Biondi, University of Pittsburgh
(Lotest Revision 18 November 1974)

16.1 INTRODUCTION

Recombination between electrons and positive ions or between positive and negative ions may proceed as a direct two-body interaction or may require the assistance of a third body, such as a neutral molecule or perhaps another electron. (Processes in which a positive or negative ion acts as the third body have not been studied; however, under circumstances of interest one expects such processes to be of lesser importance.) As we shall see, much of our quantitative information concerning recombination rates has been obtained from experiment; however, in a number of cases theoretical estimates are all we have for the rate of a particular recombination process. Probably the most extensive experimental work has been devoted to studies of two-body recombination processes, especially dissociative electron-ion recombination, with substantial work on collisional-radiative electron-ion recombination. (At moderate to high plasma densities, electrons act as third bodies in the latter reaction.) Three-body, neutral-stabilized electron-ion recombination has been studied experimentally and little more than estimates of the rate of such recombination have been made theoretically. In the case of ion-ion recombination there are some experimental data concerning both two-body (mutual neutralization) and neutral-stabilized, three-body recombination. However, only a few cases of interest have been studied; thus appeal will also be made to theoretical calculations for estimated rates. A discussion of electron-ion and ion-ion recombination processes of importance in the upper atmosphere has been given in a review (Reference 16-1).

The principal recombination reactions we shall deal with may be placed in the following simplified classifications:

A. Electron-Ion

1. Two-Body

a. Dissociative $XY^+ + e \rightarrow X + Y$ (16-1)

1. Two-Body (Cont'd.)

   b. Radiative† $X^+ + e \rightarrow X^* + h\nu$ (16-2)

2. Three-Body

   a. Electron-Stabilized† $X^+ + e + e \rightarrow X^* + e$ (16-3)

   b. Neutral-Stabilized $X^+ + e + M \rightarrow X^* + M$ (16-4)

B. Ion-Ion

1. Two-Body

   a. Mutual Neutralization $X^+ + Y^- \rightarrow X + Y$ (16-5)

2. Three-Body

   a. Thomson (neutral-stabilized) $X^+ + Y^- + M \rightarrow X + Y + M$ (16-6)

In following sections the rates of specific reactions of interest are presented and pertinent factors relating to the reliability of the measurements and/or theoretical calculations are discussed.

16.2 METHODS OF MEASUREMENT AND ANALYSIS

With the possible exception of merged-beam and certain shock-tube measurements, determinations of recombination coefficients start with the appropriate continuity equation for the electrons or ions under study.†† Using electrons as an example, we have, at a given point in space:

$$\partial n_e / \partial t = \sum_i P_i - \sum_j L_j - \nabla \cdot \vec{\Gamma}_e , \quad (16\text{-}7)$$

where P_i represents the rates of various processes leading to electron production (e.g., photoionization), L_j represents the rates of

† These two reactions taken together comprise the "Collisional-Radiative" recombination process, i.e., A.1.b and A.2.a.

†† In the case of varying electron or ion "temperature" during the measurements, it is necessary to use the full Boltzmann Transport Equation in the analysis.

16-24) has a differentially-pumped mass spectrometer been used to identify the ions present, although in one the mass spectrometer could only be operated at pressures lower than those used in the actual recombination studies (Reference 16-7).

Weller and Biondi (Reference 16-24) determined the values of $\alpha(NO^+)$ at gas temperatures of 200, 300, and 450 K from "single-pulse-afterglow" studies of electron-density decays in photoionized NO-Ne mixtures. At all temperatures conditions were achieved where NO^+ was the only significant afterglow ion, and ion "tracking" of the electron-density decays was satisfactory. Good fits of the electron decays to computer solutions of Equation (16-10) suggested very good ($\lesssim \pm 10$ percent) accuracy in the determinations. The values obtained were (7.4 ± 0.7), $(4.1^{+0.3}_{-0.2})$ and $(3.1 \pm 0.2) \times 10^{-7}$ cm^3/sec at 200, 300, and 450 K, respectively.

Except at low temperatures, where Weller and Biondi found that it required considerable care to achieve conditions which limited the concentration of the dimer ion ($NO \cdot NO^+$), the results were in good agreement with those of Gunton and Shaw (Reference 16-7), whose earlier studies using similar photoionization and microwave techniques had not involved mass-spectrometer operation under recombination-controlled (high-pressure) conditions. Their values were (10^{+5}_{-4}), $(4.6^{+0.5}_{-1.3})$ and $(3.5^{+0.5}_{-0.5}) \times 10^{-7}$ cm^3/sec at 196, 298, and 358 K, respectively. The 196 K value is almost certainly high owing to the interference of the dimer ion, whose recombination rate is discussed below.

Earlier studies by Doering and Mahan (Reference 16-5) of photoionized NO using Langmuir probes to determine the positive ion densities had led to estimates of the recombination coefficient at 300 K lying between 2×10^{-9} cm^3/sec, from the stationary-ion-density method, Equation (16-14), and 4×10^{-7} cm^3/sec, from analysis of repetitive-afterglow decay data, using Equation (16-12), with $f \leq 4$.

Much better success in obtaining consistent results between the stationary-ion-density method and a time-variation method (in this case, rate of growth measurements) has been obtained by Young and St. John (Reference 16-6), who employed chemionization in N and O atom mixtures to produce NO^+ ions. Using ionization-chamber charge-collection techniques to determine ion densities, they obtained $\alpha = (5 \pm 2) \times 10^{-7}$ cm^3/sec at 300 K, in satisfactory agreement

with the results of Weller and Biondi (Reference 16-24), and of Gunton and Shaw (Reference 16-7). At the present time, negative-ion accumulation effects in the stationary-state method have not been evaluated.

Van Lint and Wyatt (Reference 16-25) reported microwave afterglow measurements on He-NO mixtures (1000:1), ionized by a pulse of energetic (Mev) electrons. Over the mixture pressure range ~10 to 100 torr they obtained $\alpha \approx 5 \times 10^{-7}$ cm^3/sec, independen of pressure at 300 K. Rather impure NO samples were used in these studies, as evidenced by anomalously large attachment losses.

The several room-temperature measurements appear to support the value $\alpha(NO^+) = (4.1 \pm 0.3) \times 10^{-7}$ cm^3/sec, independent of the means of generating the NO^+.

Two recent experimental studies have been carried out concerning the variation of $\alpha(NO^+)$ with electron temperature. Walls and Dunn (Reference 16-26) noted the depletion in trapped NO^+ ion concentration when an electron beam of controlled energy traversed the trapping region, and determined the recombination cross-section as a function of electron energy for NO^+ ions presumably in the v 0 level of the ($X^1\Sigma^+$) ground electronic state. Huang, Biondi, and Johnsen (Reference 16-27) employed the microwave heating apparatus of Mehr and Biondi (Reference 16-21) with some minor improvements to determine $\alpha(NO^+)$ vs T_e in NO (~1 mtorr) - Ar(~10 torr) afterglows. The combined photoionization of NO by H (Lyα) and Penning ionization of NO by Ar metastables resulted in NO^+ ions which were in the ground electronic state ($X^1\Sigma^+$) and probably the v=1 or v=0 vibrational level during the measurements.

The results of the several measurements are plotted in Figure 16-2. All three of the experimental results shown are in satisfactory agreement in the range T_e 200 - 500 K, but the microwave afterglow measurements above 500 K indicate a $T_e^{-(0.37 \pm 0.03)}$ variation, while the trapped ion measurements suggest a $T_e^{-\left(0.83^{+0.16}_{-0.08}\right)}$ variation up to ~5000 K and somewhat less variation above that temperature. At present, we cannot satisfactorily account for these rather different variations between the afterglow and the trapped-ion results in terms of the possible differences in vibrational level of NO^+ in the two studies.

Results of theoretical calculations by Bardsley (Reference 16-28) and by Michels (Reference 16-29) are also shown in Figure 16-2. Bardsley calculated the contribution to $\alpha(NO^+)$ resulting from formation of the($B^2\Pi$) and the($B'^2\Delta$) repulsive states of NO^* and obtained a lower limit for (NO^+). Michels used configuration-interaction calculations

of the wave functions and potential-energy curves to determine the repulsive curves, concluding that the ($^2\Sigma^+$) and ($B^2\Pi$) states were important for electron capture by NO^+ ($v=0$) ions. While the two theories disagree by a factor of ~2.5 (the approximate uncertainty in Michels' calculation of the initial capture step), they both indicate $\sim T_e^{-0.5}$ temperature dependence over the whole energy range. Until the reasons for the discrepancies among the various determinations

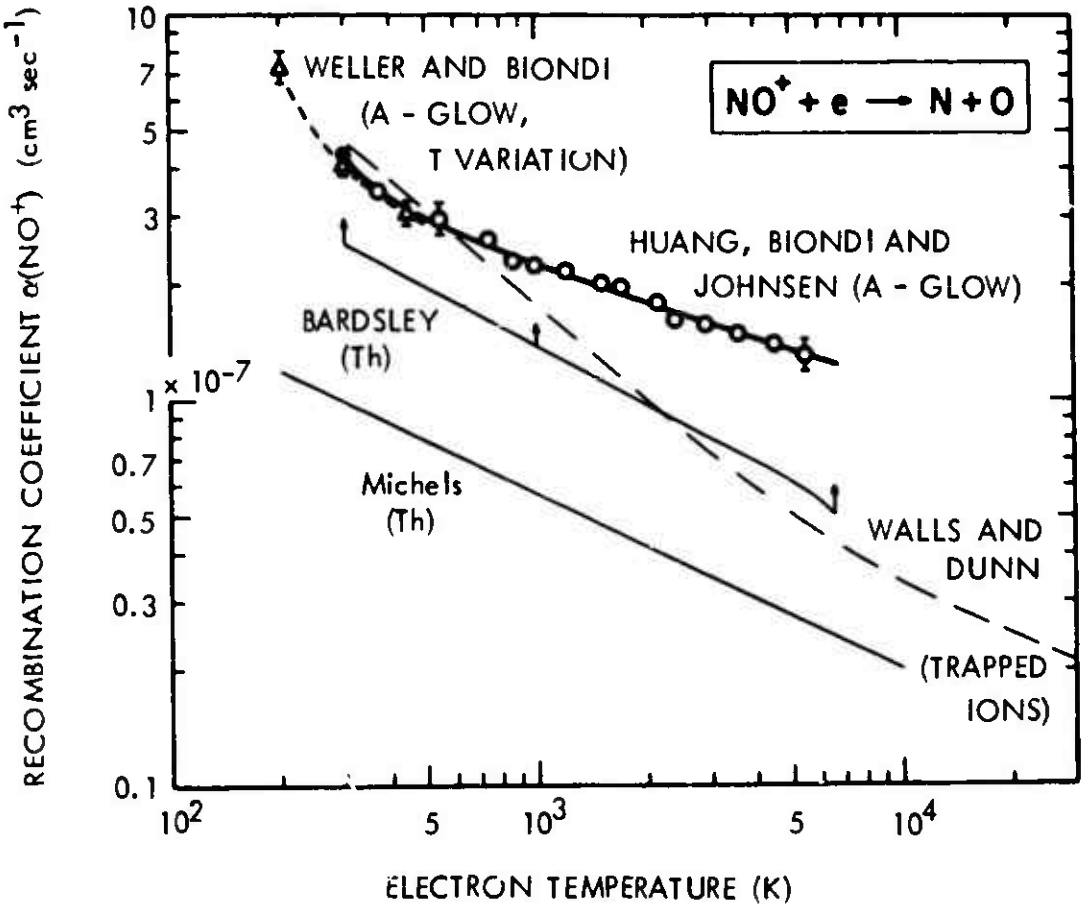

Figure 16-2. Two-body electron-ion recombination coefficient $\alpha(NO^+)$ as a function of electron temperature. Experimental results are from Weller and Biondi (Reference 16-24), Walls and Dunn (Reference 16-26), and Huang, Biondi, and Johnsen (Reference 16-27). Theoretical curves are from Bardsley (Reference 16-28) and Michels (Reference 16-29).

can be clarified it is suggested that the value $\alpha(NO^+) = (4.2 \pm 0.2) \times 10^{-7} (T_e/300)^{-(0.50 \pm 0.15)}$ cm^3 sec^{-1} be used over the range 300 - 5000 K.

Finally, as in the case of nitrogen it has been possible to obtain a value for the recombination of the dimer ion ($NO \cdot NO^+$) by increasing the partial pressure of NO to ~0.2 torr in the NO-Ne mixtures. From such studies Weller and Biondi (Reference 16-24) find $\alpha(NO \cdot NO^+) = (1.7 \pm 0.4) \times 10^{-6}$ cm^3/sec at T = 300 K.

O_2^+, O_4^+

Simultaneous microwave and mass-spectroscopic measurements of electron and positive-ion decays in oxygen-neon mixtures have been used by Kasner and Biondi (Reference 16-30) to determine $\alpha(O_2^+)$. A "single-pulse-afterglow" method was used to avoid negative-ion accumulation effects and it was found that, in contrast to earlier repetitive pulse-afterglow studies (Reference 16-31), the O_2^+ ion wall current accurately "tracked" the recombination-controlled electron-density decay. At 300 K, a value $\alpha(O_2^+) = (2.2 \pm 0.5) \times 10^{-7}$ cm^3/sec was found from $1/\langle n_e \rangle$ versus t plots exhibiting linear regions, $f \geq 10$ over the ranges $3 \times 10^{-4} < p(O_2) < 10^{-2}$ torr and $p(Ne) \approx 20$ torr. In these studies it is possible that the $^3P_2$ neon metastables produce O_2^+ ions in their ground electronic state and a high vibrational state ($v \geq 20$) or even in the first excited electronic state ($a\,^4\Pi_u$). In triple mixture (Ne:Ar:O_2) studies, attempts were made to limit the O_2^+ ions to the ground electronic and lower ($v \leq 5$) vibrational states.

Mehr and Biondi (Reference 16-21) have used a microwave afterglow/mass-spectrometer apparatus employing microwave electron heating to determine $\alpha(O_2^+)$ in oxygen-neon mixtures. Good O_2^+ ion tracking of the electron-density decays was obtained and accurate values of $\alpha(O_2^+)$ were determined from comparison of the experimental data with computer solutions of Equation (16-10). At T_e = 300 K a value $\alpha(O_2^+) = (1.95 \pm 0.2) \times 10^{-7}$ cm^3/sec was obtained, in good agreement with Kasner and Biondi's results.

Previous microwave afterglow work without mass identification of the ions by Biondi and Brown (Reference 16-16) and by Mentzoni (Reference 16-32) led to values of $\alpha \approx 3 \times 10^{-7}$ and 2×10^{-7} cm^3/sec, respectively, at low pressures (≈ 2 torr) of pure oxygen. However, at even lower oxygen pressures in oxygen-helium mixtures Kasner, Rogers, and Biondi (Reference 16-31) found substantial O_3^+ ion concentrations, so that the afterglow ionic compositions in the studies without mass analysis are in doubt.

In temperature-dependence studies Kasner and Biondi (Reference 16-30) find that, over the range 205 to 690 K, $\alpha(O_2^+)$ for ions in the ($X^2\Pi_g$) ground state decreases from the value 3.0×10^{-7} to 1.0×10^{-7} cm^3/sec. These results are shown by the X-symbols and dashed line in Figure 16-3. Similarly, Smith and Goodall (Reference 16-33) have used a Langmuir probe to determine electron-density decays in oxygen-helium afterglows; however, although mass analysis of the ions had been employed in related ion-molecule reaction studies, they omitted such analysis in the recombination work. (They

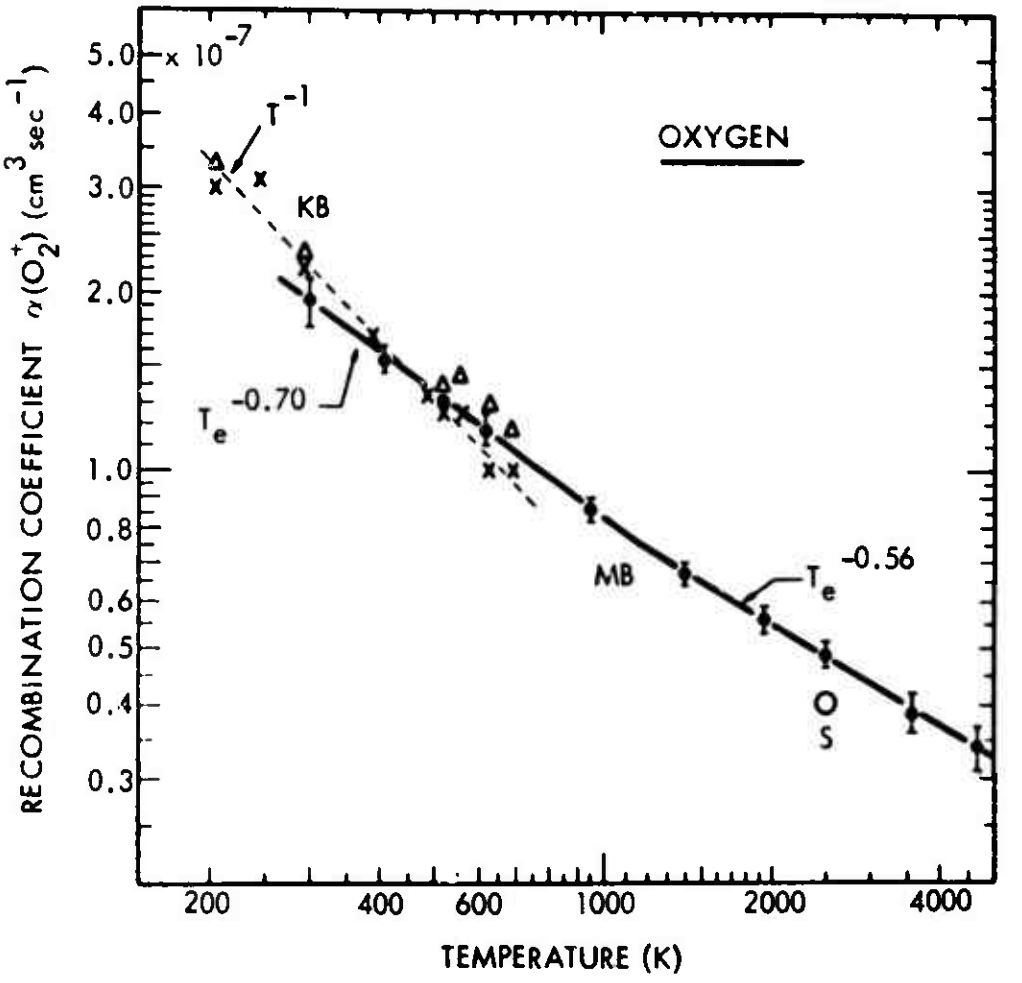

Figure 16-3. Two-body electron-ion recombination coefficient $\alpha(O_2^+)$ as a function of temperature. The experimental results are from Kasner and Biondi (KB) (Reference 16-30), Mehr and Biondi (MB) (Reference 16-21), and Sayers (S) (Reference 16-34).

are remedying this deficiency). While their value at 300 K is in good agreement with the data of Kasner and Biondi, the variation with gas temperature is less rapid. Similarly Mentzoni's data (Reference 16-32), taken over the range 300-900 K, fall consistently higher than Kasner and Biondi's results at the higher temperatures. As a result of lack of ion identification in the studies of Smith and Goodall and of Mentzoni, their inferred temperature variation of $\alpha(O_2^+)$ is probably less reliable.

Mehr and Biondi (Reference 16-21) determined $\alpha(O_2^+)$ over the range 300 K $< T_e \leq$ 5000 K (with $T_+ = T_{gas} = 300$ K) and found that the recombination coefficient varies approximately as $T_e^{-0.70}$ between 300 and 1200 K, and as $T_e^{-0.56}$ between 1200 and 5000 K. Sayers (Reference 16-34), using a Langmuir-probe/mass-spectrometer apparatus to study oxygen-helium afterglows, reported the value $\alpha(O_2^+) = 4 \times 10^{-8}$ cm^3/sec at $T_e = 2500$ K, in fair agreement with the results of Mehr and Biondi. The various data are given in Figure 16-3 and it will be seen that, over the common temperature range, $\alpha(O_2^+)$ exhibits roughly the same energy variation when T_e alone and when T_e and T_i together are increased above room temperature, provided binary mixture (O_2:Ne) data are compared. In this case, there may be some effect of excited ($a\,^4\Pi_u$) O_2^+ ions on the recombination determinations. Only in the triple-mixture studies (Ne:Ar:O_2) of Kasner and Biondi (X-symbols in Figure 16-3) can one assume that the O_2^+ ions are in their ground electronic state.

Finally, at low temperatures Kasner and Biondi (Reference 16-30) were able to separate the effects of O_2^+ and O_4^+ on the recombination loss of electrons, and found a value $\alpha(O_4^+) \sim 2.3 \times 10^{-6}$ cm^3/sec at 205 K for the dimer ion.

Zipf (Reference 16-35) has measured the branching ratios for production of various O-atom states. For each O_2^+ ion recombined, two O atoms are produced in the ratios 1.0(^{3}P) : 0.9(^{1}D) : 0.1(^{1}S).

Hydronium Series and Other Ions

Although measurements have been carried out in other gases of possible ionospheric interest (e.g., NO_2), lack of ion identification makes reporting the deduced recombination coefficients speculative. In general, at 300 K the "lighter" diatomic molecular ions (including Ne_2^+) yield α values in the range (2-5) $\times 10^{-7}$ cm^3/sec, while the more complex ions, judging by the behavior of N_4^+, $(NO \cdot NO^+)$, and O_4^+, may exhibit substantially larger values, i.e., $\alpha > 10^{-6}$ cm^3/sec.

Of particular importance, in view of its discovery in D-region rocket sounding, is the hydronium-ion series, $H_3O^+(H_2O)_n$, where n=0, 1, 2, ... A considerable amount of activity has focused upon laboratory determination of the corresponding recombination rates. In earlier studies, Green and Sugden (Reference 16-36) used a mass spectrometer to measure the decay of H_3O^+ ions from a hydrogen-oxygen-acetylene flame at approximately 2100 K, and found a value $\alpha(H_3O^+) \sim 2 \times 10^{-7}$ cm^3/sec. Wilson and Evans (Reference 16-37) used microwave techniques to measure the decay of electron density behind shock fronts in argon containing small amounts of oxygen and hydrocarbon (e.g., acetylene). Presumably the ion in these recombination-controlled decays is H_3O^+. They found that α varied approximately as T^{-2} over the range 2400 K < T < 5600 K, with a value $\alpha \simeq 1.5 \times 10^{-7}$ cm^3/sec at 3000 K. With the usual inverse temperature dependences encountered for dissociative recombination, a value in excess of 10^{-6} cm^3/sec at 300 K is implied.

Leu, Biondi, and Johnsen (Reference 16-38) have reported measurements of hydronium-series ion coefficients using their microwave-afterglow mass spectrometer apparatus. Using varying amounts of water vapor in helium buffer gas and varying the gas temperature to control the members of the hydronium-series ions present in the afterglow, they were able to study one or two of the ion types at a time. They found recombination coefficients ranging from $\alpha(19^+) = (1.0 \pm 0.2) \times 10^{-6}$ cm^{3}sec^{-1} at T=540 K to $\alpha(127^+) = (10 \pm 2) \times 10^{-6}$ cm^{3}sec^{-1} at 205 K. In addition, only a weak temperature dependence is seen in the studies of $\alpha(55^+)$ at 540, 415, and 300 K. The inferred temperature dependence, $\sim T^{-0.2}$, is weaker than that found for dissociative recombination, suggesting that for these complex ions, the very large recombination coefficients may result from excitation of internal modes (e.g., rotation) in the initial capture step, thus lengthening the autoionization time and assuring stabilization by dissociation.

Other ions of interest which have very recently been studied include HCO^+ (Reference 16-39) and the $NH_4^+(NH_3)_n$ cluster series (Reference 16-40). It is found that under conditions where $T_e = T_- \simeq T_n$ these afterglow studies indicate that $\alpha(HCO^+) = (3.3 \pm 0.5)$ and $(2.0 \pm 0.3) \times 10^{-7}$ cm^{3}sec^{-1} at 205 and 300 K, respectively, while $\alpha(NH_4^+) \simeq (1.3 \pm 0.3) \times 10^{-6}$, $\alpha[NH_4^+(NH_3)] = (2.4 \pm 0.4) \times 10^{-6}$, and $\alpha[NH_4^+(NH_3)_2] = (2.8 \pm 0.4) \times 10^{-6}$ cm^{3}sec^{-1}, at 300 K.

Theoretical Calculations

Substantial progress in theoretical calculations of dissociative recombination coefficients has been achieved in the past few years. In addition to the previously mentioned calculations by Bardsley of $\alpha(NO^+)$ (Reference 16-28) and its variation with T_e and with T_i, there are calculations by Wilkins and by Warke of $\alpha(N_2^+)$ and $\alpha(O_2^+)$ for ions in their ground vibrational states (References 16-41, 16-42), which yield values in qualitative agreement with the experimental data at 300 K. All of these calculations either make assumptions or use spectroscopic data in an effort to characterize the potential curve crossings in the direct dissociative process and are not, therefore, ab initio theoretical calculations.

Nielsen and Berry (Reference 16-43) have carried out ab initio calculations of the potential curves of the Rydberg states of the H_2 molecule which may contribute to a special form of the "indirect" dissociative recombination process, and have found that to reach the vibration continuum of one of the Rydberg states so that dissociation can occur, the H_2^+ ions must be in their v = 7 vibrational state. Thus it appears that this mechanism does not provide a significant contribution to the overall dissociative recombination process.

A difficulty with ab initio calculations of the direct dissociative process appears to be lack of a suitable technique for calculation of the repulsive potential curves of the excited molecule in the region where they cross the molecular-ion state.

16.3.1.2 RADIATIVE RECOMBINATION

Most of the available information concerning rates of radiative capture of electrons by positive ions comes from theory (References 16-44, 16-45). The radiative process (Equation 16-2) will only be of importance when the molecular-ion atomic-ion ratio is small ($< 10^{-4}$) and when charged-particle densities are low ($< 10^5$ cm^{-3}). Theory indicates that for capture into the lower levels of the excited atom, the partial recombination coefficient varies as $T_e^{-0.5}$, while for capture into the highly excited states lying within $\approx kT_e$ of the continuum, it varies approximately as $T_e^{-1.5}$. The overall recombination coefficient varies approximately as $T_e^{-0.7}$. The calculated recombination coefficients for various positive ions appear to be quite similar in magnitude, varying by less than a factor of two in going from H^+ to F^+. The dependence of the radiative recombination coefficient on electron temperature for He^+ or H^+ ions is shown in Figure 16-4 by the intercepts at the low-electron-density end of the scale, illustrating the $\approx T_e^{-0.7}$ dependence. The little experimental evidence relating to radiative recombination supports the calculated magnitude of the coefficients.

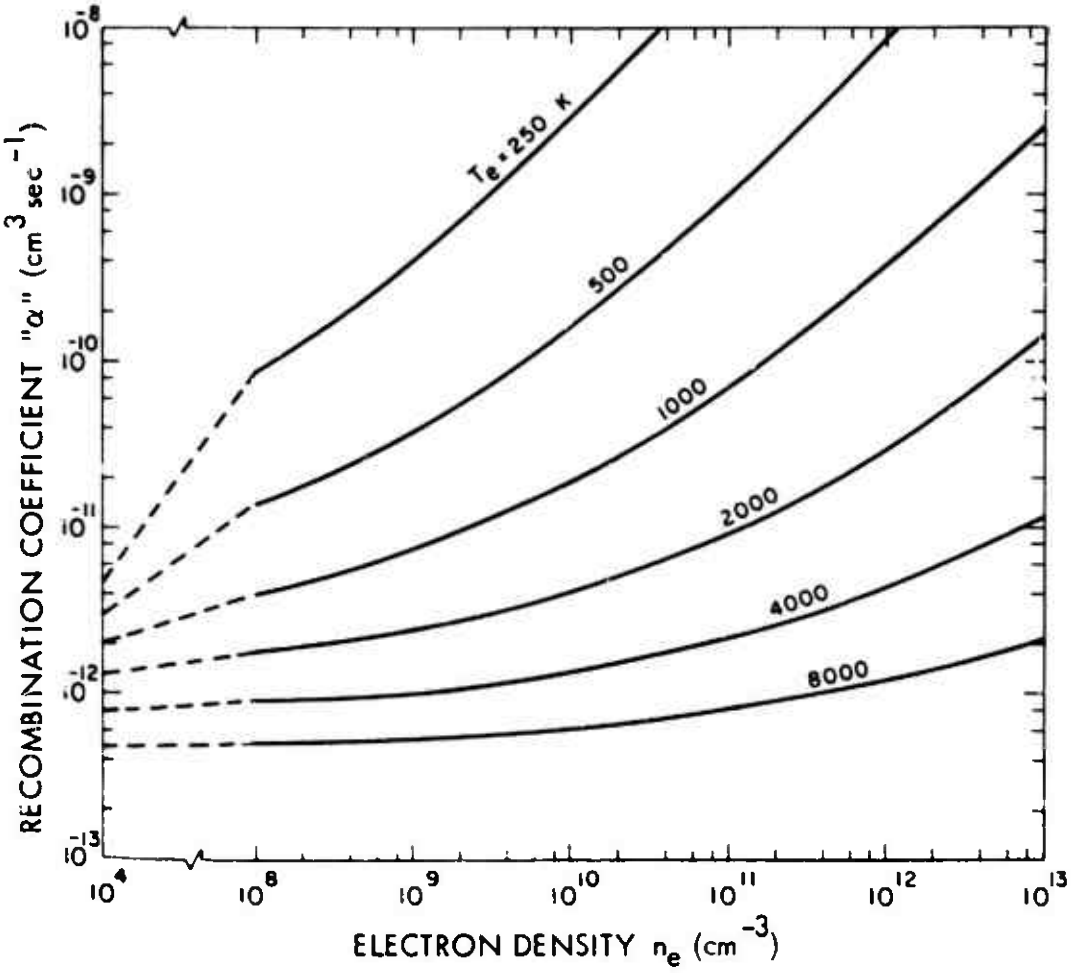

Figure 16-4. Effective two-body recombination coefficient for collisional-radiative recombination of electrons and H^+ ions as a function of electron density, over a range of electron temperatures.

16.3.2 Electron-Ion Recombination— Three-Body Processes

16.3.2.1 ELECTRON-STABILIZED RECOMBINATION

Under circumstances where a relatively large electron density ($\geq 10^6$ cm^{-3}) is present, capture of an electron by an atomic ion is assisted by a second electron (Equation 16-3), leading to the "collisional" part of collisional-radiative recombination. Here again, more is known about the process from theoretical calculations such as those of Bates, Kingston, and McWhirter (Reference 16-46), based

on the use of certain measured collision cross-section data, than from experiment. It appears that the recombination coefficient is not particularly sensitive to the identity of the singly-charged ions, and available experimental results (References 16-47, 16-48) are consistent with the calculated values.

Essentially the same three-body coefficient k_{3e} is obtained for He^+ and H^+ ions; at "low" electron temperatures, $T_e < 2000$ K, one has a variation of k_{3e} approximately as $T_e^{-4.5}$. In comparing this three-body rate to two-body rates it is useful to note that at 300 K the equivalent two-body rate for this process is "α_{3e}" $\approx (10^{-19} n_e)$ cm^3/sec, where n_e is expressed in electrons/cm^3. The results of the calculations of the electron-stabilized recombination coefficients are shown by the lines which approach a 45-degree slope in Figure 16-4.

16.3.2.2 NEUTRAL-STABILIZED RECOMBINATION

In the lower atmosphere, where neutral-molecule concentrations are large, Reaction (16-4) may raise recombination rates above the dissociative value. There is a limited amount of experimental information concerning the rate of neutral-stabilized, three-body recombination, and available theory yields little better than a crude estimate of the possible rates. Deloche et al, and Berlande et al (References 16-49, 16-50), have studied electron loss by recombination as a function of neutral concentration in a high-pressure helium-plasma-afterglow. They used microwave interferometry techniques to determine the electron-density decay bot did not employ a mass spectrometer to analyze the ions. At low-to-moderate electron densities they find the rate coefficient to be two-body in character with respect to electrons and ions and to vary directly with the neutral helium concentration, suggesting that the process under study is:

$$He_2^+ + e + He \rightarrow \text{neutral products} . \qquad (16\text{-}15)$$

They obtain a three-body rate coefficient $k = (2.0 \pm 0.5) \times 10^{-27}$ cm^6/sec at 300 K.

On the theoretical side, Massey and Burhop (Reference 16-51) used an argument paralleling Thomson's theory for ions to suggest that for "air" ions at 300 K the coefficient may be of the order

$k_{3n} \approx 6 \times 10^{-27}$ cm^6/sec. There is no information which can be used to set error limits on this estimate; however, a distinction has been made between atoms and molecules acting as third bodies in stabilizing the recombination, owing to the fact that the molecule is more effective than the atom in removing kinetic energy at a collision with an electron as a result of the large number of low-energy vibrational and rotational states which may be excited. This factor was taken into account in the estimate of k_{3n} for "air" ions and neutral stabilizing molecules. If for some reason only atoms are present, k_{3n} may be substantially smaller. This theoretical prediction is in accord with the experimental determinations for helium, which reveal a rather smaller value of k_{3n} when atoms (helium) are the stabilizing agent.

The modified Thomson theory suggests an energy variation approximately as $T_e^{-5/2}$ for the neutral stabilized process. This leads to the general rate coefficient for any positive ion of:

$$k_{3n} \approx 1 \times 10^{-(26\pm1)} (T_e/300)^{-5/2} \text{ cm}^6/\text{sec}, \qquad (16\text{-}16)$$

where the order of magnitude of the quoted uncertainty is in doubt.

16.3.3 Ion-Ion Recombination— Two-Body Processes

16.3.3.1 MUTUAL NEUTRALIZATION*

Several studies of ion-ion mutual neutralization, Equation (16-5), have been carried out at near-thermal energies. Greaves (Reference 16-9) and Sayers (Reference 16-52) have investigated halogen ions such as I_2^+ and I^-. An afterglow technique was employed, making use of radio-frequency ($\approx$ 10 MHz) determinations of the dielectric coefficient of the ions to determine ion concentrations. Ion identification was supplied by a small, differentially-pumped mass spectrometer appended to the experimental tube (Reference 16-9). In iodine (Reference 16-9) and bromine (Reference 16-52) vapor, a coefficient $\alpha_{mn} \approx 1 \times 10^{-7}$ cm^3/sec was found at $T \approx 300$ K from curves having f values between 2 and 6. With increasing temperature from 300 to 340 K, α decreased from 1.2×10^{-7} to 1.0×10^{-7} cm^3/sec in iodine, leading to an approximate $T^{-3/2}$ dependence over this extremely limited range.

*The author wishes to thank J. R. Peterson of Stanford Research Institute for his contributions to the writing of this subsection on mutual neutralization.

Hirsh et al (References 16-53, 16-54) have carried out afterglow studies of ion-ion recombination using an r-f impedance probe to determine the ion concentrations in air-like N_2-O_2 mixtures following ionization by a pulse of MeV electrons. A differentially-pumped mass spectrometer identified the principal ions undergoing recombination as NO^+, NO_2^-, and NO_3^-. Their earlier value (Reference 16-53), $\alpha_{mn} = (4 \pm 1) \times 10^{-8}$ cm^3/sec at 300 K, was later redetermined (Reference 16-54) as $(3.4 \pm 1.2) \times 10^{-8}$ cm^3/sec, and was also indicated as referring specifically to the reaction of $NO^+ + NO_3^-$. A value of $(17.5 \pm 6) \times 10^{-8}$ cm^3/sec was obtained for $NO^+ + NO_2^-$ (Reference 16-54).

Mahan and Person (Reference 16-55) studied ionic recombination in photoionized NO-NO_2-noble gas mixtures using an apparatus which did not employ mass analysis of the ions. They argued that the ions under study were probably NO^+ and NO_2^-. A parallel-plate ionization chamber employing pulsed charge collection was used to determine ion densities in the afterglow. At low pressures, a two-body coefficient $\alpha_{mn} \approx (2 \pm 0.5) \times 10^{-7}$ cm^3/sec was obtained at 300 K from decay curves exhibiting substantial f values, i.e., > 15. Thus, the quoted error limit has more to do with uncertainties concerning the exact form of the ions' spatial distribution than with slope measurement errors.

More recently, a merged-beam apparatus has been used by a group at Stanford Research Institute to obtain mutual-neutralization cross-sections between a variety of mass-analyzed positive and negative ions over a range of center-of-mass energies from 0.1 to about 300 eV. Systems that have been investigated include $H^+ + H^-$, $N^+ + O^-$, $O^+ + O^-$, $He^+ + D^-$, $N_2^+ + O_2^-$, $O_2^+ + O_2^-$, $O_2^+ + NO_2^-$, $NO^+ + NO_2^-$, $O_2^+ + NO_3^-$, and $NO^+ + NO_3^-$ (References 16-56 through 16-64). Generally, all of the measured values of α_{mn} lie between 0.5 and 3.0×10^{-7} cm^3/sec, and all rates increase toward lower energy.

A low-energy expansion of the Landau-Zener formula for these reactions (Reference 16-59) was used to extrapolate the results to thermal energies. After Boltzmann averaging, thermal rate coefficients were obtained and reported (e.g., in (Reference 16-59) in the form:

$$\alpha_{mn}(T) = A T^{-1/2} + B + C T^{1/2} + D T \,, \qquad (16\text{-}17)$$

where the constants A , B , C, and D were derived from a least-squares fit to the measurements, and T is in K. At energies near 300 K, only the first two terms are significant.

Measurements by the same group (Reference 16-64) on $Na^+ + O^-$ yielded reaction rates similar to those of $O^+ + O^-$, in contradiction to the much larger values reported by Weiner, Peatman, and Berry (Reference 16-65). On the other hand, their results on the systems $H^+ + H^-$, $He^+ + H^-$, and $He^+ + D^-$ (Reference 16-60) agreed well with those of Harrison et al(References 16-66, 16-67), who used colliding beams inclined at 20°, over an energy range from 125 to 10,000 eV.

A multistate Landau-Zener method has been used for the calculation of neutralization cross-sections between atomic ions (Reference 16-60). The agreement with experimental data is usually within a factor of two. Values for α_{mn} (300 K) were also calculated, and exceeded 1×10^{-7} cm^3/sec in every case. Calculations of this type provide information concerning the final neutral states of the products of the reaction, which can assist in the interpretation of ionospheric phenomena (Reference 16-61). It is not clear whether these calculations can be extended to include molecular systems.

16.3.3.2 OTHER TWO-BODY PROCESSES

Other processes, such as neutralization with rearrangement of the atoms in the molecules, may well offer (Reference 16-68) recombination coefficients orders of magnitude smaller than for the mutual neutralization process; these are omitted from consideration here.

16.3.4 Ion-Ion Recombination—Three-Body Processes

16.3.4.1 THOMSON RECOMBINATION

For the case of neutral-molecule-stabilized, positive-ion-negative-ion recombination, there exist measurements of recombination rates for "air" ions, whose identity, however, has not been established. Gardner (Reference 16-69) and Sayers (Reference 16-70) have measured the coefficients of Thomson recombination, k^i_{3n}, in pure oxygen and in air, respectively, over the pressure range ≈ 0.1 to 1 atmosphere at ≈ 300 K and verified the linear dependence of k on neutral gas density predicted by Thomson's theory (Reference 16-71).

A value $k^i_{3n} \simeq 3 \times 10^{-25}$ cm^6/sec was obtained. Thus at pressures in excess of 10 torr, Thomson recombination should outweigh two-body mutual neutralization.

Similar results were obtained by McGowan (Reference 16-72) in oxygen-nitrogen mixtures; however, this was without benefit of mass identification. Mahan and Person (Reference 16-55), using the method described earlier, have carried out a systematic study of three-body ionic recombination which is thought to involve the following ionic reactions:

$$NO^+ + NO_2^- + M \rightarrow \text{neutrals}, \qquad (16\text{-}18)$$

$$NO^+ + SF_6^- + M \rightarrow \text{neutrals}, \qquad (16\text{-}19)$$

and:

$$C_6H_6^+ + SF_6^- + M \rightarrow \text{neutrals}, \qquad (16\text{-}20)$$

where the third-body M includes He, Ne, Ar, Kr, Xe, H_2, D_2, and N_2. Of greatest interest is the system, $NO^+ + NO_2^- + N_2$, where a rate constant $k^i_{3n} \simeq 2 \times 10^{-25}$ cm6/sec was obtained at 300 K. The variation of k with choice of M lay between $k = 4 \times 10^{-26}$ for He and $k = 3 \times 10^{-25}$ for Xe.

There are no experimental measurements of the temperature dependence of Thomson recombination; however, Thomson's (Reference 16-71) and Natason's (Reference 16-73) treatments lead to a predicted $T_i^{-5/2}$ variation. Thus, for atmospheric ions it may be estimated that:

$$k^i_{3n} \approx 2 \times 10^{-(25 \pm 0.5)} (T_i/300)^{-5/2} \text{ cm}^6/\text{sec} \quad . \qquad (16\text{-}21)$$

16.3.4.2 OTHER THREE-BODY PROCESSES

Fueno et al (Reference 16-74) considered a two-step ion recombination process, i.e.:

$$X^+ + N \rightleftarrows (XN)^+ \quad , \qquad (16\text{-}22)$$

followed by:

$$(XN)^+ + Y^- \rightarrow XY + N \quad (16\text{-}23)$$

the rate constant of which was calculated to be $k \approx 1 \times 10^{-26}$ cm^6/sec at 300 K, and therefore should be of lesser importance than Thomson recombination.

Finally, the associative ion-ion recombination process, that is:

$$X^+ + Y^- + N \rightarrow XY + N \quad (16\text{-}24)$$

appears (Reference 16-68) to offer a much smaller coefficient, $k \approx 10^{-27}$ cm^6/sec at 300 K, than Thomson recombination; this mechanism is neglected in the present discussion, since its importance seems highly questionable.

16.4 SUMMARY

Values for the appropriate recombination coefficients for all processes where there is either sufficient experimental and/or theoretical information, or where there is a critical need for an estimate, are contained in Table 16-1. In general, those values with larger quoted uncertainties reveal a greater degree of guesswork which has taken place in attempting to evaluate the kinetics of the process.

Table 16-1. Recombination coefficient tabulation according to the form $k = (a \pm \Delta a)(T/T_r)^{(b \pm \Delta b)}$ for the case $T_r = 300\,K$. The notation [-x] signifies 10^{-x}. The symbol {T} indicates the dependence for simultaneous variation of T_{gas}, T_i, and T_e, while the symbol $\{T_e\}$ indicates the dependence for variation of T_e alone. Units are $cm^3\ sec^{-1}$ for all two-body, and $cm^6\ sec^{-1}$ for all three-body interactions.

Process	Reactants	$a \pm \Delta a$	$b \pm \Delta b$	Remarks
1. Electron-Ion				
a. Dissociative	$N_2^+ + e$	$(2.7 \pm 0.3)[-7]$	$-(0.2 \pm 0.2)\{T\}$	See Figure 16-1 for range of validity.
		$\left(1.8^{+0.4}_{-0.2}\right)[-7]$	$-(0.39)\{T_e\}$	
[simple ions]	$NO^+ + e$	$(4.1 \pm 0.3)\ [-7]$	$-(1.0 \pm 0.2)\{T\}$	200-300 K
		$(4.2 \pm 0.2)\ [-7]$	$-(0.50 \pm 0.15)\{T_e\}$	300-5000 K
				See Figure 16-2.
	$O_2^+ + e$	$(2.1 \pm 0.2)[-7]$	$-(0.7 \pm 0.3)\{T\}$	See Figure 16-3.
			$-(0.6 \pm 0.1)\{T_e\}$	
[triatomic ions]	$CO_2^+ + e$	$(3.8 \pm 0.5)\ [-7]$	$-(0.5 \pm ?)\ \{T_e\}$	300 K. See Ref. 16-8.
	$HCO^+ + e$	$(3.3 \pm 0.5)\ [-7]$		205 K
		$(2.0 \pm 0.3)\ [-7]$	$(-0.5 \pm ?)\ \{T_e\}$	300 K $T_e = T_+ = T_n$ Afterglow

Table 16-1. (Cont'd.)

Process	Reactants	$a \pm \Delta a$	$b \pm \Delta b$	Remarks
a. Dissociative (Cont'd.)				
[dimer ions]	$N_4^+ + e$	$(2 \pm 1)[-6]$	$-(1 \pm ?)\{T\}$	See Figure 16-1.
	$(NO^+ \cdot NO) + e$	$(1.7 \pm 0.5)[-6]$	$-(1 \pm ?)\{T\}$	No temp. dependence has been determined.
	$O_4^+ + e$	$(2 \pm 0.5)[-6]$	$-(1 \pm ?)\{T\}$	Measurement at 205 K.
$[H_3O^+(H_2O)_n$ series ions]	$(19)^+ + e$	$(1.3 \pm 0.3)[-6]$	$-\left(0.2^{+0.4}_{-0.1}\right)\{T\}$	$(19)^+$, $(37)^+$, and $(55)^+$ measured at 540 K. $(37)^+$ and $(55)^+$ also measured at 415 K. $(55)^+$ and $(73)^+$ measured at 300 K. $(91)^+$, $(109)^+$, and $(127)^+$ measured at 205 K.
N.B.: These are designated by their respective mass numbers, i.e., as $(M)^+$.	$(37)^+ + e$	$(2.8 \pm 0.4)[-6]$		
	$(55)^+ + e$	$(5.1 \pm 0.7)[-6]$		
	$(73)^+ + e$	$(6.1 \pm 1.2)[-6]$		
	$(91)^+ + e$	$(7.4 \pm 1.5)[-6]$		
	$(109)^+ + e$	$(9.3 \pm 2)[-6]$		
	$(127)^+ + e$	$(10 \pm 2)[-6]$		

Table 16-1. (Cont'd)

Process	Reactants	a±Δa	b±Δb	Remarks
a. Dissociative (Cont'd) $[NH_4^+(NH_3)_n$ series ions]	$18^+ + e$ $35^+ + e$ $52^+ + e$	(1.3 ± 0.3) [-6] (2.4 ± 0.4) [-6] (2.8 ± 0.4) [-6]	?	All at 300 K; $T_e=T_+=T_n$; Afterglow
b. Radiative	H^+ thru $K^+ + e$	(3.5±1)[-12]	-(0.7±0.1)	See Figure 16-4.
c. Electron-stabilized	$H^+ + 2e$ and $He^+ + 2e$	(1 ± ?)[-19]	-(4.5±?)	Valid for T_e<2000 K.
d. Neutral-stabilized	"Air" ions + neutrals + e	(1)[-26±1]	-(2.5±?)	Rough estimate.
	$He_2^+ + e + He$	(2±0.5)[-27]	-	Measured at 300 K.
2. Ion-Ion				
a. Mutual neutralization	$I_2^+ + I^-$ $Br_2^+ + Br^-$	(1)[-7±0.5]	-(1.5±0.1)	300<T<340 K
	$H^+ + H^-$	(3.9±2.1)[-7]	-(0.45±0.05)	See Refs. 16-58, 16-60.
	$H_2^+ + D^-$	(4.7±0.7)[-7]	-(0.45±0.05)	See Ref. 16-63.

Table 16-1. (Cont'd)

Process	Reactants	a±Δa	b±Δb	Remarks
a. Mutual neutralization (Cont'd.)	$O^+ + O^-$	(2.7±1.3)[-7]	-(0.45±0.05)	See Refs. 16-60, 16-61.
	$O_2^+ + O^-$	(9.6±3.0)[-8]	-(0.45±0.05)	Unpublished work of J.R. Petersan.
	$O_2^+ + O_2^-$	(4.2±1.3)[-7]	-(0.45±0.05)	See Refs. 16-57, 16-59.
	$O_2^+ + NO_2^-$	(4.1±1.3)[-7]	-(0.45±0.05)	See Ref. 16-59.
	$O_2^+ + NO_3^-$	(1.3±0.5)[-7]	-(0.45±0.05)	See Ref. 16-62.
	$N_2^+ + O_2^-$	(1.6±0.5)[-7]	-(0.45±0.05)	See Ref. 16-57.
	$NO^+ + O^-$	(4.9±1.5)[-7]	-(0.45±0.05)	Unpublished work of J.R. Peterson.
	$NO^+ + NO_2^-$	(5.1±1.5)[-7] (1.75±0.6)[-7]	-(0.45±0.05) -(0.45±0.05)	See Ref. 16-59. See Ref. 16-54.
	$NO^+ + NO_3^-$	(8.0±3.0)[-7] (3.4±1.2)[-8]	-(0.45±0.05) -(0.45±0.05)	See Ref. 16-62. See Ref. 16-54.
	$N^+ + O^-$	(2.6±0.8)[-7]	-(0.45±0.05)	See Refs. 16-56, 16-57, 16-60.

Process	Reactants	a ± Δa	b± Δb	Remarks
b. Neutral-stabilized	"Air"	(3 ± 1)[-25	-(2.5± ?)	M = N_2, O_2 .
	$NO^+ + NO_2^- + M$	(2± ?)[-25	-(2.5± ?)	M = N_2
		(4± ?)[-26	-(2.5± ?)	M = He
		(3± ?)[-25	-(2.5± ?)	M = Xe

REFERENCES

16-1. Biondi, M. A., Can. J. Chem. 47, 1711 (1969).

16-2. Kasner, W. H., and M. A. Biondi, Phys. Rev. 137, A317 (1965).

16-3. Gray, E. P., and D. E. Kerr, Ann. Phys. (New York) 17, 276 (1962).

16-4. Frommhold, L., and M. A. Biondi, Ann. Phys. (New York) 48, 407 (1968).

16-5. Doering, J. P., and B. H. Mahan, J. Chem. Phys. 36, 669 (1962).

16-6. Young, R. A., and G. St. John, Phys. Rev. 152, 25 (1966).

16-7. Gunton, R. C., and T. M. Shaw, Phys. Rev. 140, A748, A756 (1965).

16-8. Weller, C. S., and M. A. Biondi, Phys. Rev. Letts. 19, 59 (1967).

16-9. Greaves, C., J. Electron. Control 17, 171 (1964).

16-10. Biondi, M. A., Phys. Rev. 109, 2005 (1958).

16-11. Oskam, H., Phillips Res. Repts. 13, 335 (1968).

16-12. Biondi, M. A., Phys. Rev. 129, 1181 (1963).

16-13. Kasner, W. H., Phys. Rev. 167, 148 (1968).

16-14. Conner, T. R., and M. A. Biondi, Phys. Rev. 140, A778 (1965).

16-15. Frommhold, L., and M. A. Biondi, Phys. Rev. 185, 244 (1969).

16-16. Biondi, M. A., and S. C. Brown, Phys. Rev. 76, 1697 (1949).

16-17. Faire, A. C., and K. S. W. Champion, Phys. Rev. 113, 1 (1959).

16-18. Mentzoni, M.H., J. Geophys. Res. 68, 4181 (1963).

16-19. Hackam, R., Planet. Space Sci. 13, 667 (1965).

16-20. Kasner, W.H., Phys. Rev. 164, 194 (1967).

16-21. Mehr, F.J., and M.A. Biondi, Phys. Rev. 181, 264 (1969).

16-22. Hagen, G., Air Force Cambridge Research Laboratories, Rept. AFCRL-68-0649 (1968).

16-23. Theard, L.P., Sixth Intl. Conf. Phys. Electronic Atomic Collisions, Cambridge, Mass. (1969); p. 1042.

16-24. Weller, C.S., and M.A. Biondi, Phys. Rev. 172, 198 (1968).

16-25. van Lint, V.A.J., and M.E. Wyatt, General Atomics, Rept. DASA-GA-5615, Part II (1964).

16-26 Walls, F.L., and G.H. Dunn, J. Geophys. Res. 79, 1911 (1974).

16-27. Huang, C.M., M.A. Biondi, and R. Johnsen, Phys. Rev. A, in press (1975).

16-28. Bardsley, J.N., Phys. Rev. A2, 1359 (1970).

16-29. Michels, H., United Aircraft Research Laboratories, Rept. AFWL-TR-73-288 (1974).

16-30. Kasner, W.H., and M.A. Biondi, Phys. Rev. 174, 139 (1968).

16-31. Kasner, W.H., W.A. Rogers, and M.A. Biondi, Phys. Rev. Letts. 7, 321 (1961).

16-32. Mentzoni, M.H., J. Appl. Phys. 36, 57 (1965).

16-33. Smith, D., and C.V. Goodall, Planet. Space Sci. 16, 1177 (1968).

16-34. Sayers, J., J. Atm. Terrestr. Phys. 6, Spec. Suppl., 212 (1956).

16-35. Zipf, E.C., Jr., Bull. Am. Phys. Soc. 15, 418 (1970).

16-36. Green, J.A., and T.M. Sugden, Ninth Symp. (Intl.) on Combustion, The Combustion Institute, Pittsburgh, Pa. (1963); p. 607.

16-37. Wilson, L.N., and E.W. Evans, J. Chem. Phys. 46, 859 (1967).

16-38. Leu, M.T., M.A. Biondi, and R. Johnsen, Phys. Rev. A7, 292 (1973).

16-39. Leu, M.T., M.A. Biondi, and R. Johnsen, Phys. Rev. A8, 420 (1973).

16-40. Huang, C.M., M.A. Biondi, and R. Johnsen, private communication (1974).

16-41. Wilkins, R.L., J. Chem. Phys. 44, 1884 (1966).

16-42. Warke, C.S., Phys. Rev. 144, 120 (1966).

16-43. Nielsen, S.E., and R.E. Berry, Sixth Intl. Conf. Phys. Electronic Atomic Collisions, Cambridge, Mass. (1969); p. 1047.

16-44. Seaton, M.J., Monthly Not. Roy. Astron. Soc. 119, 81 (1959).

16-45. Bates, D.R., and A. Dalgarno, in Atomic and Molecular Processes, D.R. Bates, Ed., Academic Press, New York and London (1962); Chapter 7.

16-46. Bates, D.R., A.E. Kingston, and R.W.P. McWhirter, Proc. Roy. Soc. A267, 297 (1962).

16-47. Kuckes, A.F., R.W. Motley, E. Hinnov, and J.G. Hirschberg, Phys. Rev. Letts. 6, 337 (1961).

16-48. Born, G.H., Phys. Rev. 169, 155 (1968).

16-49. Deloche, R., A. Gonfalone, and M. Cheret, Compt. Rend. Acad. Sci. Paris 267, 934 (1968).

16-50. Berlande, J., M. Cheret, R. Deloche, A Gonfalone, and C. Manus, Phys. Rev. A1, 887 (1970).

16-51. Massey, H.S.W., and E.H.S. Burhop, Electronic and Ionic Impact Phenomena, Oxford Univ. Press, London and New York (1952).

16-52. Sayers, J., in Atomic and Molecular Processes, D. R. Bates, Ed., Academic Press, New York and London (1962); Chapter 8.

16-53. Hirsch, M. N., G. M. Halpern, and N. S. Wolf, Bull. Am. Phys. Soc. 13, 199 (1968).

16-54. Eisner, P. M., and M. N. Hirsch, Phys. Rev. Letts. 26, 874 (1971).

16-55. Mahan, B. H., and J. C. Person, J. Chem. Phys. 40, 392, 3683 (1964).

16-56. Aberth, W., J. R. Peterson, D. C. Lorents, and C. J. Cook, Phys. Rev. Letts. 20, 979 (1968).

16-57. Aberth, W. H., and J. R. Peterson, Phys. Rev. A1, 158 (1970).

16-58. Moseley, J. T., W. H. Aberth, and J. R. Peterson, Phys. Rev. Letts. 24, 435 (1970).

16-59. Peterson, J. R., W. H. Aberth, J. T. Moseley, and J. R. Sheridan, Phys. Rev. A3, 1651 (1971).

16-60. Olson, R. E., J. R. Peterson, and J. T. Moseley, J. Chem. Phys. 53, 3391 (1970).

16-61. Olson, R. E., J. R. Peterson, and J. T. Moseley, J. Geophys. Res., Space Phys. 76, 2516 (1971).

16-62. Moseley, J. T., W. H. Aberth, and J. R. Peterson, Bull. Am. Phys. Soc. 12, 208 (1971).

16-63. Peterson, J. R., J. T. Moseley, and W. H. Aberth, Bull. Am. Phys. Soc. 15, 1510 (1970).

16-64. Moseley, J. T., W. H. Aberth, and J. R. Peterson, Seventh Intl. Conf. Phys. Electronic Atomic Collisions, Amsterdam, Holland (1971).

16-65. Weiner, J., W. B. Peatman, and R. S. Berry, Phys. Rev. Letts. 25, 79 (1970).

16-66. Rundel, R. D., K. L. Aitken, and M. F. A. Harrison, J. Phys. B2, 954 (1969).

16-67. Gaily, T. D., and M. F. A. Harrison, J. Phys. B3, 1098 (1970).

16-68. Bortner, M. H., General Electric Company, Rept. AFCRL-65-392 (1965).

16-69. Gardner, M. E., Phys. Rev. 53, 75 (1938).

16-70. Sayers, J. Proc. Roy. Soc. A169, 83 (1938).

16-71. Thomson, J. J., Phil. Mag. 6, 377 (1924).

16-72. McGowan, S., Can. J. Phys. 45, 429, 439 (1967).

16-73. Natason, G. L., Zhur. Tekh. Fiz. 29, 1373 (1959).

16-74. Fueno, T., H. Eyring, and T. Ree, Can. J. Chem. 38, 1693 (1960).